Enhancing the representation of water management in global hydrological models

Guta Wakbulcho Abeshu[1], Fuqiang Tian[2], Thomas Wild[3], Mengqi Zhao[4], Sean Turner[3], A F M Kamal Chowdhury[5], Chris R. Vernon[4], Hongchang Hu[2], Yuan Zhuang[2], Mohamad Hejazi[3+] and Hong-Yi Li[1*]

[1]Department of Civil and Environmental Engineering, University of Houston, Houston, 77204, US
[2]Department of Hydraulic Engineering, Tsinghua University, Beijing, 100084, China
[3]Joint Global Change Research Institute, Pacific Northwest National Laboratory, College Park, MD 20740, US
[4]Pacific Northwest National Laboratory, Richland, WA 99354, US
[5]Earth System Science Interdisciplinary Center (ESSIC), University of Maryland, College Park, MD 20740, U.S.
[+] Now at King Abdullah Petroleum Studies and Research Center (KAPSARC), Riyadh, Saudi Arabia

Correspondence to: Hong-Yi Li (hongyili.jadison@gmail.com)

Abstract. This study enhances an existing global hydrological model (GHM), Xanthos, by adding a new water management module that distinguishes between the operational characteristics of irrigation, hydropower, and flood control reservoirs. We remapped reservoirs in the Global Reservoir and Dam database to Xanthos' 0.5-degree spatial resolution so that a single lumped reservoir exists per grid cell, which yielded 3790 large reservoirs. We implemented unique operation rules for each reservoir type based on their primary purposes. In particular, hydropower reservoirs have been treated as flood control reservoirs in previous GHM studies, while here, we determined the operation rules for hydropower reservoirs via optimization that maximizes long-term hydropower production. We conducted global simulations using the enhanced Xanthos and validated monthly streamflow for 91 large river basins where high-quality observed streamflow data were available. A total of 1878 (296 hydropower, 486 irrigation, and 1096 flood control and others) out of the 3790 reservoirs are located in the 91 basins and are part of our reported results. The Kling-Gupta Efficient (KGE) value (after adding the new water management) is ≥ 0.5 and ≥ 0.0 in 39 and 81 basins, respectively. After adding the new water management module, model performance improved for 75 out of 91 basins and worsened for only seven. To measure the relative difference between explicitly representing hydropower reservoirs and representing hydropower reservoirs as flood control reservoirs (as is commonly done in other GHMs), we use normalized-root-mean-square-error (NRMSE) and the coefficient of determination (R^2). Out of the 296 hydropower reservoirs, NRMSE is > 0.25 (i.e., considering 0.25 to represent a moderate difference) for over 44% of the 296 reservoirs when comparing both the simulated reservoir releases and storage time series between the two simulations. We suggest that correctly representing hydropower reservoirs in GHMs could have important implications for our understanding and management of freshwater resource challenges at regional-to-global scales. This enhanced global water management modeling framework will allow for the analysis of future global reservoir development and management from a coupled human-earth system perspective.

1 Introduction

Reservoirs are pivotal in fulfilling various societal needs, including irrigation, hydropower production, flood control, domestic water supply, and navigation, to list a few (Belletti et al., 2020; Biemans et al., 2011; Grill et al., 2019). There are 6,862 large reservoirs ($\geq 0.1 km^3$) globally, with a cumulative storage capacity of 6,197 km^3 in the Global Reservoir and Dam (GRanD) dataset (Lehner et al., 2011). Many of these reservoirs serve multiple purposes. However, if we partition reservoirs into categories based on their primary purposes, 1,789 are irrigation reservoirs with a total storage capacity of ~1,100 km^3; 1,541 are hydropower reservoirs with a total storage capacity of ~3,880 km^3; 542 are flood control reservoirs with a total storage capacity of ~509 km^3; and the rest are water supply, navigation, or recreation reservoirs. Water storage and releases in any given reservoir are managed based on the reservoir's purposes. It is, therefore, important in Global Hydrological Models (GHMs) to represent how management strategies differ across reservoirs with different purposes in order to more accurately simulate water balances and explore the implications of alternative water management strategies. It is particularly important to distinguish the behavior of hydropower reservoirs from others because hydropower production represents the primary purpose for nearly 63% (based on GRanD) of total global reservoir storage capacity.

Hanasaki et al. (2006) proposed a generic reservoir simulation scheme for use in GHMs that has been widely used, denoted hereinafter as the *Hanasaki scheme*. This scheme categorizes all reservoirs into only two types based on their primary purposes: irrigation and non-irrigation reservoirs. All non-irrigation reservoirs are essentially simulated as flood control reservoirs. The *Hanasaki scheme* determines reservoir release in two stages. First, the provisional release is estimated. For irrigation reservoirs, the provisional release is estimated as a function of the demand for water placed on the reservoir, while provisional release from non-irrigation reservoirs is the long-term mean inflow. The provisional release is then adjusted based on the reservoir's degree of regulation (i.e., the ratio of reservoir storage capacity to inflow).

Most existing GHMs (see Table 1) adopt the Hanasaki classification and treat reservoirs as irrigation or non-irrigation (Burek et al., 2020; Hanasaki et al., 2008; Pokhrel et al., 2012; Schaphoff et al., 2018; Müller Schmied et al., 2021; Sutanudjaja et al., 2018; van der Knijff et al., 2010; Wisser et al., 2010; Zhou et al., 2020). Several GHM studies have employed this scheme with some modifications, including H08 (Hanasaki et al., 2008), MATSIRO-TRIP (Pokhrel et al., 2012), WaterGAP2 (Müller Schmied et al., 2021), WBMPlus (Wisser et al., 2010), and LPJmL4 (Schaphoff et al., 2018). For example, some studies have modified the technique for estimating the parameters for irrigation reservoirs, i.e., water demand and spatial extent of the dependent area of a specific reservoir, etc. (Biemans et al., 2011). LPJmL (Schaphoff et al., 2018) and PCR-GLOBWB (Sutanudjaja et al., 2018) estimate irrigation reservoir release based on water demand, and for all other primary purposes, these models use a default strategy where they release a pre-determined value (e.g., average discharge) while maintaining levels between a minimum and maximum storage. LISFLOOD (van der Knijff et al., 2010) and CWatM (Burek et al., 2020) do not classify reservoirs based on their purposes. Instead, they use three pre-determined releases based on storage: minimum outflow, non-damaging outflow, and normal outflow.

Most GHMs, however, still largely follow the *Hanasaki scheme* in treating all non-irrigation reservoirs as flood control reservoirs. In the *Hanasaki scheme*, the inflow, minimum pool level, maximum static full level, and water stored at the beginning of the hydrological year are the only significant factors controlling the magnitude and timing of water release (Hanasaki et al., 2006; Yassin et al., 2019). In reality, among non-irrigation reservoirs, hydropower reservoirs are typically operated differently from flood control reservoirs (Turner et al., 2017; Loucks et al., 2017). An essential difference between them is that hydropower reservoirs mostly operate with the objective of storing water over certain target levels to maximize releases through turbines (Loucks et al., 2017). The minimum and maximum releases corresponding to the minimum and maximum storage levels are also pre-determined. Furthermore, in large storage hydropower reservoirs with a large degree of regulation, storage levels may vary significantly over the course of a year (between the minimum and maximum storage levels) to avoid significant spillage and enable reliable hydropower generation throughout the year. Conversely, an essential feature of flood control reservoirs is to provide a reliable capacity to retain a predicted or unforeseen future flooding event by emptying existing reservoir storage. The objective of flood control reservoirs is to reduce peak flow magnitude, and storage level is only a concern when there is an incoming flood event (Votruba and Broza, 1989). Therefore, treating hydropower reservoirs as flood control reservoirs can significantly underestimate their operational benefits (Turner et al., 2017; Loucks et al., 2017).

The model performance implications of representing reservoirs as flood control versus hydropower reservoirs are evident at the individual reservoir level. However, there remains a gap in the literature regarding the regional-to-global model performance implications of the representation of hydropower reservoirs, given that GHMs are designed for applications at this spatial scale but have not yet explored this question surrounding the representation of hydropower (Best et al., 2011; Döll et al., 2009; Hanasaki et al., 2008; Pokhrel et al., 2012; Schaphoff et al., 2018; Wisser et al., 2010; Voisin et al., 2013). This study overcomes the aforementioned limitation by demonstrating an enhancement to how water management is employed in Xanthos, a global hydrological model. Xanthos is a relatively lightweight model designed to interact with the components of the Global Change Intersectoral Modeling System (GCIMS), which includes the Global Change Analysis Model (GCAM) (Hejazi et al., 2013, 2014; Li et al., 2017) at its core, along with a broader suite of interacting energy, water, and land models. GCAM is an integrated tool for exploring the Multi-sector dynamics of coupled human-earth systems and the response of these systems to global changes (Calvin et al., 2019). Aided by Xanthos, GCAM enables an internally consistent evaluation of time-evolving water supply (i.e., surface water, groundwater, and desalinated water) and demand dynamics across multiple sectors. As such, GCAM and Xanthos have been used in combination to study issues such as the relative contributions of humans and climate change to future global water scarcity (Graham et al., 2020), regional water scarcity (Birnbaum et al., 2022), and sub-national water scarcity (Khan et al., 2020; Wild et al., 2021b, c), as well as climate impacts on the future evolution of hydropower and the broader power sector (Arango-Aramburo et al., 2019; Santos da Silva et al., 2021). Nevertheless, the existing version of Xanthos, denoted here as *Xanthos-original*, focuses only on representing the natural global water balance without human interventions such as reservoirs (Hejazi et al., 2013; Liu et al., 2018; Vernon et al., 2019). Accounting for water

management in the way we propose will ensure that the crucial role of reservoirs is represented in regulating streamflow by mediating water availability and demand (Wan et al., 2018, 2017; Zhang et al., 2020, 2019, 2018).

The specific objectives of this study are threefold: 1) to enhance Xanthos by adding a new water management module, where irrigation, hydropower, and flood control reservoirs are treated differently (this enhanced Xanthos is denoted as *Xanthos-enhanced*); 2) to evaluate the performance of *Xanthos-enhanced* in terms of reproducing observed streamflow variability; and 3) to understand the impacts of differentiating between flood control and hydropower reservoir operations on regional-to-global scale water balance. The first two objectives represent improvements to *Xanthos* and, thus, potential improvements to a broad array of coupled human-earth system studies that rely on linkages between GCAM and Xanthos. The third objective has the potential to inform future improvements to a diverse array of GHMs (see Table 1) because our study is the first, to our knowledge, to explore the GHM performance improvements that can be gained by treating the operational characteristics of hydropower dams as distinct from those of irrigation and flood control dams.

2 Methodology

Xanthos is a distributed global hydrological model with a spatial resolution of 0.5 degrees. Xanthos is a framework that enables users to create customized configurations of potential evapotranspiration estimation, runoff generation and concentration, routing, and post-processing modules (https://github.com/JGCRI/xanthos). By accounting for reservoir operation and local water withdrawal, *Xanthos-enhanced* enables exploring the influence of water management (Fig. 1). This section focuses on the water management module but first briefly summarizes the runoff and river routing components for completeness. For more details on the runoff and river routing components, please refer to Li et al. (2017), Liu et al. (2018), and Vernon et al. (2019).

2.1 Runoff Generation Module

Runoff generation in *Xanthos-original* is based on the ***abcd*** model. First developed by Thomas (1981), ***abcd*** is a simple water balance model effective for capturing key hydrologic processes, and their interactions, in diverse climatic and landscape settings (Martinez and Gupta, 2010, 2011). Liu et al. (2018) introduced the ***abcd*** model into Xanthos as its runoff module, simulating direct runoff, baseflow, evapotranspiration, and soil moisture at a monthly time step. The sum of direct runoff and baseflow is denoted as total runoff, which feeds into the river routing module. The five parameters in the ***abcd*** model are described in Table 2. Parameters ***a*** and ***b*** pertain to runoff characteristics, while ***c*** and ***d*** relate to shallow soil moisture and deeper groundwater storage. The fifth parameter is a snowmelt coefficient, denoted as ***m***. Since *Xanthos-original* is a distributed model, each grid cell has its own set of ***abcd*** parameters, though these parameters can optionally have the same values for all grid cells within a given river basin. Xanthos classifies the global water system into 235 large water basins.

2.2 River Routing Module

In Xanthos, the routing of water through river networks is simulated using a simple cell-to-cell river routing scheme, a modified version of the River Transport Model (Branstetter and Erickson, 2003), hereinafter denoted as MRTM. MRTM is essentially based on the linear reservoir routing method. The channel flow rate is estimated as a function of channel water storage, channel velocity, and flow distance from one grid cell to another (Zhou et al., 2015). MRTM uses spatially variable but temporally constant channel velocities, which were derived by averaging the long-term channel velocity simulations from Li et al. (2015). The flow distance values were derived by tracing the natural dominant river channel between grid cells to account for the meandering nature of rivers (Wu et al., 2011). Here we add a channel velocity adjustment coefficient (Table 2) to account for the uncertainties in our channel velocity field. For more details about MRTM, please refer to Zhou et al. (2015).

2.3 Water Management Module

To enhance Xanthos, we add a water management module on top of the river routing module. The water management module represents the two most common surface water management activities: local surface water extraction and reservoir operation. Local surface water extraction is water that is locally consumed within a particular grid cell. For example, some fraction of the water applied to irrigated agricultural land may evaporate and effectively become unavailable for use in a given grid cell. This local consumptive water use is subtracted from the total runoff produced by the ***abcd*** model. The remaining runoff is discharged into the channels and routed downstream using MRTM. If the consumptive water use is greater than the total runoff in a grid cell, the remaining runoff is zero. In such a case, the grid cell is considered to have unmet water demand or access to supply from other external sources, such as desalination or groundwater pumping, which are not currently represented in Xanthos. If there is a reservoir in a grid cell, local runoff (after removing water consumption) and upstream inflow are first intercepted and stored in the reservoir. Reservoir operation is then invoked to estimate the release from the reservoir to the downstream grid cells. Note that a grid cell can contain only one reservoir. That is, if there are multiple individual reservoirs co-located in the same grid cell, we first lump these individual reservoirs into a single reservoir with a storage capacity equivalent to all the combined reservoirs. The primary purpose of this lumped reservoir within a given grid cell is determined in two steps: 1) sum up the storage capacities of the individual reservoirs in four categories based on their primary purposes (irrigation, hydropower, flood control, and other); 2) in each category, sum up the reservoir storage capacities. The aggregated reservoir's primary purpose is assigned to the category with the largest summed storage capacity, while the volume of the single lumped reservoir is equivalent to the sum of all individual reservoir storage capacities across all purposes. The reservoir operation rule is defined for each lumped reservoir based on its primary purpose. For reservoir purposes, if the estimated release is unavailable or less than 10% of the mean annual inflow, the monthly release is set to the minimum environmental flow requirement, i.e., 10% of the mean annual inflow (Tennant, 1976; Hanasaki et al., 2008; Müller Schmied et al., 2021). Next, we provide more details on the operating rule for each reservoir type (Fig. 1).

2.3.1 Irrigation Reservoirs

Irrigation reservoirs are represented by adapting the widely adopted Hanasaki et al. (2006) approach, which determines the reservoir release based on the upstream inflow and the total water demand from the downstream areas. More specifically, for each irrigation reservoir, the provisional release is given as

$$R'_{m,y} = \begin{cases} \frac{i_{mean}}{2} * \left(1 + \frac{d_{m,y}}{d_{mean}}\right), & d_{mean} \geq 0.5 * i_{mean} \\ i_{mean} + d_{m,y} - d_{mean}\,, & d_{mean} < 0.5 * i_{mean}\,, \end{cases} \quad (1)$$

where $R'_{m,y}$ is the provisional monthly reservoir release (m^3/s) in month m and year y; $d_{m,y}$ is the monthly mean total water demand from the downstream areas that are dependent on this reservoir (m^3/s); d_{mean} is the long-term mean monthly water demand from the downstream areas (m^3/s); and i_{mean} is the mean annual inflow from upstream (m^3/s). Both the magnitude of long-term average water demands and the monthly timing of demands are used as inputs, so releases are responsive to the timing of typical demands. The *Hanasaki scheme* has an allocation coefficient, which is a coefficient for grid cells with more than one reservoir upstream, but here it is assumed to be one and is thus not shown in equation (1). This is because, in this study, the dependent areas of reservoirs on the same stream do not overlap.

Though deterministic by nature, the provisional release equation for irrigation reservoirs is demand-driven. $d_{m,y}$ is calculated based on the delineated downstream dependent grid cells. If d_{mean} is greater than or equal to 50% of the mean annual inflow i_{mean}, 50% of i_{mean} is continually released as a baseline, while seasonal release dynamics are determined by the ratio of monthly demand to d_{mean}. If d_{mean} is less than 50% of i_{mean}, the provisional release can be estimated as the mean annual inflow modified by the seasonal demand variation around the mean annual demand.

The provisional release is further adjusted based on the degree of regulation ($\boldsymbol{\gamma}$), initial storage at the beginning of y^{th} operational year ($S_{first,y}$), and reservoir capacity reduction factor ($\boldsymbol{\alpha}$). The degree of regulation is the ratio of reservoir storage capacity (C) to annual total inflow in cubic meters per year (I_{mean}). The reservoir capacity reduction factor is a non-dimensional constant that reduces the total reservoir capacity reported in GRanD to account for surcharge storage and storage reduction due to sediment accumulation. It ranges between 0~1, where a lower value means the reservoir capacity may have been significantly reduced by sediment accumulation, and at 0, the reservoir is not operational. The final release is estimated as follows:

$$R_{m,y} = \begin{cases} \left(\frac{S_{first,y}}{\alpha C}\right) * R'_{m,y} & \gamma \geq 0.5 \\ \left(\frac{\boldsymbol{\gamma}}{0.5}\right)^2 * \left(\frac{S_{first,y}}{\boldsymbol{\alpha} C}\right) * R'_{m,y} + \left(1 - \left(\frac{\boldsymbol{\gamma}}{0.5}\right)^2\right) i_{m,y} & 0 \leq \gamma < 0.5, \end{cases} \quad (2)$$

where $R_{m,y}$ is the monthly release (m^3/s); $i_{m,y}$ is the monthly inflow (m^3/s); and I_{mean} is the annual inflow (m^3/year).

The GRanD reservoirs can be classified into relatively large and small storage reservoirs based on the degree of regulation. If a reservoir's total storage capacity is less than 50% of its mean annual inflow, it is considered a hydrologically small reservoir, whereas greater than 50% indicates a hydrologically large reservoir. In relatively large reservoirs (upper part of equation 2),

releases are relatively independent of their monthly inflows, while in relatively small reservoirs (lower part of equation 2), releases are dependent on their monthly inflows (Hanasaki et al., 2006).

The total water demand for each reservoir is estimated by summing up water demand values from grid cells within the reservoir's downstream dependent area. The reservoir-dependent area is determined following Hanasaki et al. (2006), Haddeland et al. (2006), and Biemans et al. (2011). Specifically, the downstream spatial extent of reservoir dependency along the main stem is determined based on an average stream velocity and the study's temporal interval (monthly). Assuming an average velocity of 0.5 m/s, the total travel distance of water in one month is 0.5 m/s × (30 × 24 × 3600 s/month) × (0.001 km/m) = 1296 km/month. Therefore, the dependent downstream grid cells along the main stem are roughly 20 grid cells (0.5 × 0.5 degrees, about 55 km along each direction) downstream. If other reservoirs are located within this travel distance, we assume the dependency on the current reservoir stops and is taken over by the other reservoir (the allocation coefficient in Hanasaki et al. (2006) is set to one for this reason). We then delineate a buffer zone within four–grid-cell ranges from each side of the main stem. Finally, assuming water movement is by gravity only, those grid cells with a mean elevation lower than that of the reservoir are identified as the reservoir's dependent grid cells within the buffer zone.

2.3.2 Hydropower Reservoirs

We represent the operation of hydropower reservoirs using a stochastic dynamic programming (SDP) approach (Loucks et al., 2017; Turner et al., 2017). The SDP approach extends the dynamic programming approach to account for the uncertain nature of reservoir inflows explicitly (Loucks et al., 2017). It executes sequential decisions for temporal stages with nonlinear objectives while considering reservoir inflows as random variables (Loucks et al., 2017). For a known inflow $i_{m,y}$ and hydrologic state variables in the current period (Stedinger et al., 1984), the SDP formulation estimates the benefit function, $f_{m,y}$, resulting from each release decision $R_{m,y}$ as,

$$f_{m,y}(S_{m,y}, i_{m,y}) = max_{R_{m,y}} E\{B_{m,y}(S_{m,y}, i_{m,y}, R_{m,y}) + f_{m+1,y}(S_{m+1,y}, i_{m,y})\} \quad \forall S_{m,y}, i_{m,y} \;\; m \in \{1, \dots, T\}, \tag{3}$$

where T is the current system period (T = 12 for a monthly operating scheme). The reservoir state at each decision-making time step, i.e., month m in the year y, is described by the storage $S_{m,y}$ and the current inflow $i_{m,y}$. For each state and time step, the release decision $R_{m,y}$ is selected to maximize the immediate benefit $B_{m,y}(S_{m,y}, i_{m,y}, R_{m,y})$ plus future benefit function $f_{m+1,y}(S_{m+1,y}, i_{m,y})$, which depends on the resultant state of the system at time step $m + 1$, i.e., the succeeding month.

The method for simulating the hydropower reservoir operation is adopted from ***reservoir***, an R package that contains several reservoir release decision-making tools, including the SDP techniques described above (Turner, 2016). The same method was also employed in a global-scale study of hydroelectric plants' vulnerability to climate change (Turner et al., 2017). We integrated the SDP approach from this package (Turner, 2016; Turner et al., 2017) into Xanthos for hydropower release simulation. Here the SDP approach is first trained using the naturalized inflow to each reservoir to represent hydrological uncertainty, which we obtain by running MRTM without the water management option. The objective function is set to

maximize hydropower production over the long term. The SDP procedure is executed to develop an energy-maximizing release policy for each month as a function of storage levels (see Fig. 1).

The working concept for the SDP algorithm we implemented is summarized as follows. Power (P in kilowatt) generated by a hydropower plant is given by $P = \eta\rho g*R*H$, where ρg is the specific weight of water (kN/m^3), R is turbine flow (m^3/s), H is the turbine head (m), and η is efficiency (a constant value of 0.9 is used in this study). ρg term is a constant term; hence the power generation variability is a function of $R*H$. Thus, maximizing the $R*H$ translates to maximizing power production. The following four steps are used to identify an optimal policy (i.e., a hydropower-maximizing policy) from a given reservoir inflow realization. First, we discretize the maximum turbine flow (i.e., the maximum allowable flow rate through the turbine) into ten increments (i.e., between 0 to maximum turbine flow) and the storage capacity into 1000 (i.e., between 0 to storage capacity) increments. Discretization of decision and state variable space is a common practice in implementing dynamic programming-based methods (Piccardi and Soncini-Sessa, 1991; Zeng et al., 2019). Second, we developed a depth-volume relationship based on an assumed reservoir shape. Here we assume a wedge reservoir shape for all reservoirs globally in the absence of any global datasets to support more heterogeneous representations. The storage-volume relationship is employed to estimate storage depth (y) corresponding to 1000 discretized storage volume levels. The turbine head at each storage level was obtained from the sum of y and intake elevation. The intake elevation is computed as the maximum turbine head (i.e., the difference between reservoir pool level and turbine elevation) minus the maximum storage depth (equal to dam height in this study). Using the power equation, the maximum turbine head is computed from the plant installed capacity and maximum turbine flow. Third, we have an array of releases and turbine heads from the discretization; multiplying them as a matrix yields a *1000x10* matrix of *RH* (i.e., ten possible *RH* values for each storage level). In the present study, we select the policy that maximizes power generation. The best policy for each month (i.e., January to December) at all 1000 storage levels is obtained through backward recursive iterations (i.e., from December to January)—this yields what we call *the release policy*, a matrix of size 1000 (storage levels) x 12 (months). Lastly, during streamflow simulation, the storage volume and month are used to look up the optimal release policy table (i.e., the *1000x12* table), and the corresponding optimal release is determined. When a storage level is at the reservoir's maximum storage capacity, release equals the maximum turbine flow that generates power at the power plant's installed capacity.

While the online integration of SDP with hydrological models brings considerable advantages, it also presents certain challenges. One such challenge is managing the uncertainties of inflow data, as these directly influence the reservoir's operational policy. The effects of inflow uncertainty can lead to potential operational deviations, such as preemptive release of water due to overestimated inflows, or undue conservation based on underestimated inflows. To lighten this challenge, a careful parameter selection process is implemented (see section 2.4). The initial stage of this process prioritizes achieving a reliable long-term water balance that aligns closely with observations. By focusing on this balance, we aim to minimize the uncertainties inherent in the inflow data, thereby improving the reliability of operational decisions derived from the SDP model.

2.3.3 Flood Control and Other Purpose Reservoirs

The primary purpose of flood control reservoirs is to redistribute the floodwater from a flood season to a non-flood season. The operation of flood control reservoirs is also estimated following Hanasaki et al. (2006).

$$R_{m,y} = \begin{cases} \left(\frac{S_{first,y}}{\alpha C}\right) * i_{mean} & \gamma \geq 0.5 \\ \left(\frac{\gamma}{0.5}\right)^2 \left(\frac{S_{first,y}}{\boldsymbol{\alpha} C}\right) * i_{mean} + \left(1 - \left(\frac{\gamma}{0.5}\right)^2\right) i_{m,y}, & 0 \leq \gamma < 0.5, \end{cases} \quad (4)$$

where $R_{m,y}$ is the monthly release (m^3/s); and $i_{m,y}$ is the monthly inflow (m^3/s). In this study, release from reservoirs categorized as "others" is also determined as a function of inflow and storage characteristics only and is thus similar to flood control reservoirs. The logical reasoning for the equations employed here is in line with equation (2). For instance, as with irrigation reservoirs, the $\boldsymbol{\alpha}$ and $\boldsymbol{\gamma}$ parameters are used to adjust the behavior of flood control reservoirs.

2.4 Model Parameter Determination Strategy

In total, *Xanthos-enhanced* now includes seven parameters the runoff and routing/water management modules. Typically, there are two strategies for determining the parameter values in a hydrologic model: calibration and estimation *a priori* (i.e., without calibration) (Beven, 2012). Parameter calibration requires thousands of model runs and is only feasible for computationally inexpensive models. Feasibility can be compromised by parameter calibration efforts that require refactoring a model to run more efficiently, the budget required to scale simulations via high-performance computing resources, and the time needed for a comprehensive run. Furthermore, most hydrological models are subject to concerns surrounding equifinality, since the number of parameters, in most cases, far exceeds the number of observational variables available for calibration (Beven, 2006). Alternatively, parameter estimation *a priori* requires each parameter to be physically meaningful and have robust relationships with the existing climate or landscape information. These relationships are usually not readily available and have to be identified via sound prior knowledge (e.g., Li et al., 2015) or machine-learning techniques (e.g., Abeshu et al., 2022; Li et al., 2021).

This study proposes a new, two-stage parameter determination strategy (described in Fig. 2) that seeks to overcome existing limitations by (1) screening out parameter sets that are not physically meaningful and (2) significantly reducing the overall computational burden associated with identifying optimal parameter sets. We seek to determine seven Xanthos parameters in total: five from the runoff module and two from the routing module, including water management. We determine runoff parameters in the 1st stage and routing parameters in the 2nd stage. The runoff module runs separately from the routing and water management modules and is relatively lightweight, taking a standard personal computer less than two hours to execute it at a global scale for one million simulations covering a 20-year duration. Meanwhile, the routing and water management modules are much more computationally intensive because they run at a three-hour time step to ensure numerical stability (Li et al., 2011, 2015). The 1st stage takes advantage of the lightweight runoff module to exhaustively explore the runoff parameter space before handing off favorable subsets of parameters to the 2nd stage, which then limits its focus to the

more computationally intensive search for the remaining two (routing) parameters. We describe the parametrization strategy in detail in the remainder of this section, whereas the results of implementing the strategy using a particular set of global data are detailed in Section 3.2. This strategy is designed based on the characteristics of the Xanthos modules, but we suggest that it has the potential to be useful in diverse global hydrological modeling contexts.

In the first stage, we determine the optimal values for the five parameters in the runoff generation module (see Table 2) in four steps. 1) We generate one million runoff parameter combinations using a Latin Hypercube Sampling (LHS) scheme (McKay et al., 1979)(Fig. S1). LHS is a statistical method for multidimensional parameter space sampling. The stratified sampling strategy employed by LHS ensures that all portions of the sampling space are represented (McKay et al., 1979). The user decides on the required number of parameter combinations and individual parameters' upper and lower bounds. Based on that, LHS simultaneously stratifies all input dimensions. 2) For each runoff parameter combination, we execute the runoff module to produce the simulated monthly total runoff time series at each grid cell in the study period. In this study, we uniformly apply the same parameter values to all the grid cells in a basin to generate monthly runoff time series at each grid cell. Parameter values vary among basins, just not across grid cells within a basin. 3) We calculate the simulated annual runoff depth at each grid cell. We then take the spatial average across the grid cells within the upstream drainage area of a gauge station where observed streamflow data is available, denoted as Q_{sim_annual} (mm/year). 4) At the river gauge station, we calculate the long-term mean of observed streamflow and divide it by the drainage area, Q_{obs_annual} (mm/year). We then select the top 100 runoff parameter combinations that produce the smallest normalized root mean square error (NRMSE) between (Q_{sim_annual} – annual water consumption) and Q_{obs_annual}.

Before these 100 runoff parameter combinations are passed onto the 2nd stage, the runoff generated by the top 100 parameters is further evaluated at the mean monthly scale to confirm that the selected parameter combinations yield reasonable runoff simulations in terms of timing. For this purpose, we compare the peak time of the simulated mean monthly runoff (i.e., the calendar month when the mean monthly runoff is highest, denoted as simulated peak runoff time hereinafter) with that of Global Runoff Data Center (GRDC) mean monthly flow (i.e., the calendar month when the mean monthly flow is highest, denoted as observed peak flow time) (Fig. S2). Note that the mean monthly runoff employed here is a simple spatial average with no channel routing. Therefore, a reasonable simulated peak runoff time is expected to be earlier than the observed peak flow time by 0~3 months. The range of 0~3 months is estimated by applying a 1.0 m/s travel velocity to the longest river in the world, the Nile River, which yields a total travel time between 2.0 and 3.0 months.

The selected 100 parameter combinations are then passed on to the 2nd stage, where we determine the final optimal parameter set in four steps. 1) We set the reservoir capacity reduction factor ($\boldsymbol{\alpha}$) to a value of 0.85 following Hanasaki et al. (2006). 2) Channel velocity adjustment coefficient ($\boldsymbol{\beta}$) is sampled in a relatively uniform manner within the range of 0.1~10.0. In total, there are 19 possible $\boldsymbol{\beta}$ values to be considered, i.e., $\boldsymbol{\beta}$ = 0.1, 0.2, 0.3, 0.4, 0.5, 0.6, 0.7, 0.8, 0.9, 1.0, 2.0, 3.0, 4.0, 5.0, 6.0, 7.0, 8.0, 9.0, 10.0. 3). For each of the 100 selected runoff parameter combinations, we use the corresponding simulated runoff time series as the inputs and run the river and water management modules 19 times (each time corresponds to one of the 19 $\boldsymbol{\beta}$ values and $\boldsymbol{\alpha}$ = 0.85) at a 3-hour time step. 4) We validate the simulated streamflow time series at the grid cell where

the gauge station is located against the observed monthly streamflow time series. From Step (3), there are 1900 simulations for each basin, each corresponding to a combination of five runoff parameters and one routing parameter (***a***, ***b***, ***c***, ***d***, ***m***, and ***β***). The final optimal parameter set is the one that produces the best model performance (per the performance metrics discussed in the following Section 2.5). Note that, within each basin, we held the set of parameters constant across the cells, which is a reasonable simplification since, typically, there is no sufficient observational data to effectively capture the spatial heterogeneity of these parameters within each basin.

This new strategy has several benefits. First, it largely alleviates the equifinality issue by effectively sampling the whole parameter space. Our experimental design covers the full theoretical value range for each of the six parameters. Second, it reduces the computational burden to a reasonable level. Our suggested approach includes one million model runs for the runoff module at the monthly time step for each river basin and another 1900 runs for the river routing and water management modules at the three-hour time step. We suggest that this new strategy applies to those hydrologic modeling frameworks where 1) some module(s) is computationally much cheaper than the others and 2) these modules must run sequentially instead of simultaneously. A demonstration of this parameter determination strategy is provided in Section 3.

2.5 Metrics for Model Assessment

To evaluate model performance, we use the Kling–Gupta efficiency (KGE) (Gupta et al., 2009), which is given by

$$KGE = 1 - \sqrt{(r-1)^2 + \left(\frac{\sigma_{Sim}}{\sigma_{Obs}} - 1\right)^2 + \left(\frac{\mu_{Sim}}{\mu_{Obs}} - 1\right)^2}, \quad (5)$$

where $\sigma_{sim}, \sigma_{obs}, \mu_{sim}, and\ \mu_{obs}$ are the standard deviation of streamflow value for a given simulation, the standard deviation of observed streamflow, the simulated mean, and the observed mean values, respectively. A higher KGE indicates a better degree of agreement between the simulated and observed variables, and a KGE value of 1.0 indicates perfect agreement. The KGE value is -0.41 if the simulated monthly flow equals the observed long-term mean flow for all months (Knoben et al., 2019).

While KGE is a useful means of evaluating the skill of a particular set of model parameters in reproducing observed streamflow, we also wish to directly compare simulation outputs against one another across multiple model configurations and parameterizations for both reservoir storage and reservoir release. To enable this comparison, we employ the following indices that capture key aspects of reservoirs' regulation behavior.

Reservoir Impact Index (RII): RII is the ratio of a reservoir storage capacity (C) in m^3 to annual mean flow (Q_{mean}) (López and Francés, 2013; Wang et al., 2017). RII is similar to the *Hanasaki scheme*'s degree of regulation term, except that RII is computed at the GRDC site instead of the reservoir site. Low and high values of RII indicate that the stream is lightly and heavily regulated, respectively.

$$RII = \frac{C}{Q_{mean}} \quad (6)$$

Where Q_{mean} is the observed annual mean flow at the GRDC site in m^3/year.

Seasonality Index (SI): SI represents the degree of variability in monthly release or storage within a year and is computed with the Walsh and Lawler (1981) method.

$$SI = \frac{1}{\bar{X}} \sum_{m=1}^{12} \left| X_m - \frac{\bar{X}}{12} \right| \quad (7)$$

Where X_m is the mean monthly value for the month m and $\bar{X}$ is the annual mean value. SI ranges between 0 and 1.833, indicating uniform distribution over the 12 months and a single-month occurrence, respectively. When applying this equation, use units that represent a measure of water quantity over a month, such as depth (e.g., mm/month) or volume (e.g., m^3/month).

Coefficient of Variation (CV): CV is the ratio of standard deviation to mean and is employed here to depict the extent of inter-annual variability in storage and release.

No reliable global observational datasets exist for reservoir storage levels and releases, so it is difficult to establish whether the metric values (for RII, SI, and CV) from one model configuration versus another are closer to reality. Despite this limitation, comparing metric values across simulations is still useful to understand the effects of modeling assumptions (e.g., representing hydropower reservoirs as such instead of as flood control reservoirs). To enable comparison, we measure the difference or closeness between two alternative time series, representing two alternative model configurations or parametrizations, using normalized-mean-square-error (NRMSE) and coefficient of determination (R^2). NRMSE typically captures the magnitude difference between two-time series, while R^2 measures the proportion of the variance explained (Moriasi et al., 2007).

2.6 Metrics for Sensitivity Analysis

As we have discussed, equifinality is a crucial issue when calibrating a hydrological model that is highly parameterized. To assess model robustness, it is important to evaluate how sensitive the model's performance is to each model parameter. The sensitivity analysis approach we propose here is moderately different from traditional methods since we implement a novel parameter determination strategy (see Section 2.4). The sensitivity analysis aims to identify the most and least influential model parameters. Such understanding can help identify priorities of parameter estimation in future works and simplify or improve the model structure. Two separate sensitivity analyses are performed. The first sensitivity analysis is performed before parameter selection using results from all one million parameter sets. Here, an NRMSE for each of the one million parameter sets was computed between simulated annual runoff and observed annual runoff. The annual runoff is observed as annual streamflow converted to an equivalent depth over the upstream contributing basin area. The simulated annual runoff is calculated by subtracting the basin's annual water consumption from the total runoff. The correlation coefficient was then computed between an array of the computed NRMSE and each runoff parameter to evaluate the correlation between the change in parameter values and model performance. We computed five correlation coefficients from the one million runs, i.e., between model performance and the five runoff parameters for each basin.

After applying the new parameter selection strategy, the second sensitivity analysis is carried out on 1900 samples (i.e., samples generated from combining the 100 samples from the first stage with 19 discretized $\boldsymbol{\beta}$ values). Each sample includes the five runoff parameters and the velocity adjustment coefficient employed for streamflow simulation during the second stage. Here, the model performance (KGE) is computed between the monthly observed and simulated streamflow. We switched to KGE for monthly time series evaluation as we are interested in metrics that reflect the agreement in both magnitude and patterns of monthly flow. The correlation coefficient is computed between the KGE and each parameter. We obtain six correlation coefficient values for each basin, corresponding to the five ***abcd*** model parameters and the routing parameter (i.e., $\boldsymbol{\beta}$). As with its interpretation in Stage 1 of the sensitivity analysis, here, a higher correlation coefficient between a parameter's values and the corresponding performance metric (in this case, KGE) suggests that the variance in model simulation outcomes is more strongly related to the changes in the target parameter, hence more sensitive to this parameter.

3 Global Application and Results

We apply *Xanthos-enhanced* over the global domain at a 0.5-degree resolution and monthly time step. The study period is 1971-1990 based on the availability of forcing and observed streamflow data over all the basins. We divide the study period into a calibration period, 1971-1980, and a validation period, 1981-1990.

3.1 Data and Numerical Experiments

For this study, we obtain gridded global monthly climatic data, including precipitation, maximum temperature, and minimum temperature, from the WATer and global CHange (WATCH; Weedon et al., 2011) dataset, which covers the period 1971-2001. We obtain global reservoir data from the GRanD dataset (Lehner et al., 2011) (Fig. 3a). Monthly water demand and consumptive water use data for various sectors at a 0.5-degree resolution are from (Huang et al., 2018b, a), which are available from 1971 to 2010 (Fig. 3c). Observed streamflow data for model parameter identification and validation are obtained from the GRDC (https://www.bafg.de/GRDC). We begin by comparing Xanthos' corresponding MRTM upstream area (after locating each gauge station within a Xanthos grid cell) with the GRDC gauge contributing area. If the drainage area difference is larger than ±20%, we look for an option to readjust the station to one of the eight neighbouring grid cells. Here, only gauges within ±20% in area difference (3097 GRDC gauges) are retained for further use in this study. Temporal filtering of these gauges with the availability of 20 years (1971-1990) of continuous data reduced the number of stations to 1178. These gauge stations are located within 91 of the 235 Xanthos basins. For model validation purposes, we select the GRDC gauge with the largest upstream area within each basin, i.e., 91 GRDC gauges in total (Fig. 3b).

The GRanD database we use here only considers reservoirs with storage capacity values greater than 0.1 km^3. We also exclude reservoirs with missing storage capacity values and those identified with purposes such as tide control, which reduces the total GRanD reservoirs from 6862 to 6847. For any grid cell with more than one reservoir, we aggregate all of the reservoirs located locally (i.e., within the grid cell) into a single reservoir with a storage capacity equivalent to that of the local

reservoirs combined. The purpose of the combined storage is determined by the two steps described in Section 2.3. As a result of this process, the 6847 GRanD reservoirs are remapped into 3790 reservoirs. Among the 3790 reservoirs, 1095, 598, and 2097 are categorized as irrigation, hydropower, and flood control and others, respectively (Fig. 1). Furthermore, out of the 3790 global reservoirs, only 1878 of them are located within the 91 basins simulated in this study. Out of these 1878 reservoirs, the primary purpose is hydropower for 296, irrigation for 486, and flood control/others for 1096. The reservoirs across these 91 basins make up approximately 66% of the total dams within the GRanD dataset. The construction years of these dams pose a critical factor in deciding the calibration-starting year. Here, we found that ~ 69.5% of these dams were constructed before 1971 and an additional ~17.2% were built between 1971 and 1981. We considered it reasonable to include all dams, regardless of their construction year, in the calibration starting from 1971 mainly for two reasons: i) incrementally aggregating dams built during this period over time, in addition to the dams built before 1971, would significantly complicate the modeling process, and ii) dams constructed before 1981 account for approximately 84% of the total storage within these basins.

With the aforementioned data, we carry out three global simulations to explore the performance of the *Xanthos-enhanced* (see Table 3): 1) A simulation with *Xanthos-original*, denoted as *Xanthos-original-sim*, where the simulated flow is obtained by routing calibrated runoff data generated by Liu et al. (2018) with calibrated ***abcd*** model parameters but no water management; 2) A simulation with *Xanthos-enhanced* denoted as *Xanthos-enhanced-sim*, where we run the runoff, river routing, and water management modules with the final optimal parameter values determined following the new strategy as outlined in Section 2.4; 3) A simulation similar to *Xanthos-enhanced-sim*, but treating all the hydropower reservoirs as flood control reservoirs, denoted as *Xanthos-enhanced-sim2*. By comparing *Xanthos-enhanced-sim* with *Xanthos-original-sim*, we demonstrate the overall improvement of model performance from *Xanthos-original* to *Xanthos-enhanced* due to a combination of the new parameter determination strategy and new water management module. Note that in Liu et al. (2018), the traditional, brute-force calibration strategy was invoked since *Xanthos-original* only consists of a monthly runoff generation module and runs very quickly. By comparing *Xanthos-enhanced-sim* with *Xanthos-enhanced-sim2*, we isolate the net difference between simulating hydropower reservoirs based on Eqn. (3) and the traditional approach employed by GHMs, i.e., treating hydropower reservoirs as flood control reservoirs based on Eqn. (4).

3.2 Parameter Determination Outcomes

We apply the two-stage model parameter determination strategy described in Section 2.4 using the global datasets described in Section 3.1. The LHS generates a parameter set using defined bounds (see supplementary Fig. S1). Here, we describe the results from the implementation of the two-stage strategy using the Amazon basin as an example. A subset of one hundred good parameter sets (filtered) are identified among the one million parameter sets (raw) (see supplementary Fig. S2a). The mean monthly runoff generated with the subset and the observed mean monthly runoff (see supplementary Fig. S2b) showed that the simulated runoff peak time is earlier than the streamflow peak time, within the 1-3 month range established in Section 2.4. The model's integrity is contingent upon the theoretical expectation of the streamflow peak trailing the runoff peak by a

span of days to months. Any set of parameters resulting in a reversed pattern, where the runoff peak occurs later, are deemed unacceptable due to possible anomalies within the model.

The peak time differences (i.e., the difference between GRDC mean monthly peak flow time minus simulated runoff peak flow time) corresponding to the selected sets of parameters are among the best of the one million samples when ranked in an ascending order based on an absolute value of the peak time difference (supplementary Fig. S2c). The robustness of the implemented procedure is justified by the presence of a range of parameter values between their upper and lower bounds (see supplementary Fig. S2d), indicating that the selected parameters are not concentrated within a specific parameter space. These characteristics have also been observed in most of the basins evaluated for this study (figure not shown). We select one parameter combination for each basin that results in the best KGE value. The spatial maps of the final optimal parameter values are shown in supplementary Fig. S3. In most cases, optimal values for parameter ***a*** are close to the upper bound, while those of parameter ***d*** is closer to the lower bound. Parameter ***b*** is low in basins in the high-latitude sub-region; to some degree, this may be attributed to the fact that, in general, evapotranspiration decreases towards most of the high-latitude regions. Parameter ***c*** seems to be lower in the eastern hemisphere and has relatively no distinct pattern in the western hemisphere basins. The snowmelt parameter ***m*** is only above zero in regions with significant snow contributions. The parameter $\boldsymbol{\beta}$ is higher in high-latitude basins. $\boldsymbol{\beta}$ was only introduced to readjust the global velocity data after noticing bias in monthly flow timing at many sites; hence applications of our methodology that use more reliable velocity data should consider setting $\boldsymbol{\beta}$ to a value of 1. The high values of $\boldsymbol{\beta}$ in the higher latitude basins could be attributed to the original velocity estimation approach's systematic bias in cold regions (Li et al., 2015).

3.3 Global Evaluation

Overall, Xanthos' performance has improved after adding the water management module. Figure 4 shows violin plots of KGE between the GRDC monthly observed streamflow and those simulated from the *Xanthos-original-sim* and *Xanthos-enhanced-sim* simulations for the 91 basins during the calibration (Fig. 4a) and validation (Fig. 4b) periods, respectively. In most cases, during both calibration and validation periods, the *Xanthos-enhanced-sim* simulation's KGE values are consistently higher than those of the *Xanthos-original-sim* simulation. For the *Xanthos-enhanced-sim* simulation, the KGE value is no less than 0.5 and 0.0 for 59/39 and 89/81 basins during the calibration/validation period, respectively.

Figure 5 provides a comprehensive comparison of the *Xanthos-enhanced-sim* and *Xanthos-original-sim*, emphasizing the impact of water management integration. This is illustrated both spatially, through a map depicting KGE differences, and temporally, via time series plots for selected basins. Overall, by incorporating this element, improvements are noticeable in the KGE values of 75 basins - indicating a better simulation accuracy for these basins. The increase in KGE values is substantial, exceeding 0.05 when compared to those of the Xanthos-original-sim. However, it is also crucial to note that water management integration negatively affected the KGE values (i.e., KGE values decreased by more than 0.05) in seven basins. In the remaining nine basins, KGE did not significantly change. For basins in which performance worsened, the decrease in

performance is likely due to factors such as the uncertainties in the climate forcing data and GRDC streamflow observations (Moges et al., 2021) and the lack of spatial heterogeneity in the estimated parameters at the sub-basin scale (i.e., the parameters are uniform across all grid-cells in a given basin). The distribution and operational patterns of reservoirs, particularly in relation to their closeness to gauge stations, could also represent a nontrivial contributing factor to this issue.

To further examine Xanthos' performance in more detail, Fig. 5 also shows the monthly time series of simulated and observed streamflow at the 12 GRDC stations (out of the 91 evaluated here) with relatively higher average annual water demand in their geographical region (see Fig. 3c) and hence stronger water management effects. The twelve basins are Rhine, Po, Siberia North Coast, Ziya He Interior, Ganges-Brahmaputra, Chao Phraya, Murray-Darling, South Africa South Coast, Uruguay-Brazil South Atlantic Coast, East Brazil South Atlantic Coast, California Basin, and Mid Atlantic. Compared to *Xanthos-original*, *Xanthos-enhanced-sim* better captures the seasonal variations of streamflow, more closely matching the observed streamflow during the high-flow and low-flow periods. This highlights the importance of the reservoir regulation effect (e.g., attenuating high flows and augmenting low flows) that *Xanthos-original* has not captured.

3.4 Parameter Sensitivity Analysis

To identify which parameters are most critical (i.e., contribute most to variance in key model outputs), we evaluate the sensitivity of the model's performance to the changes of $\boldsymbol{a}$, $\boldsymbol{b}$, $\boldsymbol{c}$, $\boldsymbol{d}$, $\boldsymbol{m}$, and $\boldsymbol{\beta}$, as shown in Fig. 6. Note that we fix the value of $\boldsymbol{\alpha}$ at 0.85 following Hanasaki et al. (2006) in this study. We first carry out the sensitivity analysis on the runoff parameters based only on the first-stage parameter determination results (Fig. 6a). The results show a significant sensitivity (correlation coefficient > |± 0.4|) only for parameters $\boldsymbol{a}$ (which represents the propensity of runoff to occur before the soil is fully saturated) and $\boldsymbol{b}$ (which represents an upper limit on the sum of evapotranspiration and soil moisture storage). The correlation between parameter $\boldsymbol{a}$ and model performance is negative, indicating it is inversely related to the NRMSE computed from annual observed and simulated runoff. Parameter $\boldsymbol{a}$ controls the amount of runoff generation when soil is under saturated, and the relationship suggests annual runoff is estimated better when saturation excess runoff is not the primary process. Parameter $\boldsymbol{b}$ controls the soil saturation level. Hence, it is responsible for the memory of the basin. Therefore, the positive correlation indicates that the difference between simulated and observed annual runoff increases as the basin memory increases.

A similar analysis is made for the set of parameters generated by combining the one hundred best ***abcd*** model parameters set with the velocity adjustment parameter ($\boldsymbol{\beta}$) (Fig. 6b). Here, it appears that $\boldsymbol{\beta}$ has a stronger influence on model performance than the other parameters. This is expected because the differences among the 100 selected runoff parameter combinations are supposed to be small (e.g., see supplementary Fig. S2a (filtered) for Amazon basin). For $\boldsymbol{\beta}$, the sensitivity corresponds to adjustment in flow timing, leading to improved KGE. Note that this parameter can be avoided with a better estimate of spatially and temporally varying flow velocity. Considering these observations, it becomes evident that enhanced parameterization of this variable, along with the other variable used to estimate the grid's water residence time (i.e., channel

length), warrants increased attention. Hence, in future proper generation and integration of these components are crucial for boosting the model's accuracy and robustness; given their pivotal role in the MRTM flow routing process.

3.5 Hydropower Reservoirs

Among the 91 basins we studied here, 51 have one or more hydropower reservoirs included in GRanD and hence in our simulations. Recall that these reservoir counts reflect our lumping of multiple reservoirs together within any given grid cell, so 296 reservoirs in our methodology reflect 433 actual reservoirs. At each of the 296 reservoirs, the simulated release and storage time series from *Xanthos-enhanced-sim2* are compared with those from *Xanthos-enhanced-sim* to identify the benefit of capturing hydropower operations.

Figure 7 compares *Xanthos-enhanced-sim* and *Xanthos-enhanced-sim2* with regard to intra-annual (Fig. 7a and b) and inter-annual (Fig. 7c and d) variability. The Seasonality Index (SI) summarizes the intra-annual variability; weak seasonality (i.e., low SI) indicates that most months contribute significantly to the annual magnitude, and strong seasonality (i.e., high SI) indicates that very few months contribute to the annual flux magnitude. Although SI showed more difference, both the SI and Coefficient of Variation (CV) (which summarizes inter-annual variability) for release fall on the 1:1 line for most reservoirs (Fig. 7a and c), indicating that in most cases, the two scenarios have less impact on the intra- and inter-annual variability of release. On the other hand, both SI and CV values for storage at most reservoirs show a significant difference, indicating that the two experiments significantly disagree in inter-annual and intra-annual variability of storage. We emphasize that the significant takeaway from this comparison is not that one experiment's storage and release simulations are more variable than the other but that the two experiments led to substantially different seasonal and annual patterns. This highlights the drawbacks of representing hydropower reservoirs as flood control reservoirs.

Figure 8 summarizes the reservoir storage and release comparisons between *Xanthos-enhanced-sim* and *Xanthos-enhanced-sim2* with an empirical Cumulative Distribution Function (CDF) that plots R^2 (and/or NRMSE) values across all 296 hydropower reservoirs according to their rank-ordered exceedance probabilities. The spatial map for the comparisons is also shown in Fig. S4. Recall that a high NRMSE value means a significant magnitude difference between the two different time series, and a low R^2 value means a significant timing difference. Of the 296 reservoirs, the simulated reservoir releases significantly differ between the two model configurations in ~ 45 % of reservoirs in terms of magnitude (if we set a threshold at NRMSE > 0.25) (Fig. 8b) and at only ~28% in terms of timing (if we set a threshold at $R^2 < 0.5$) (Fig. 8a). According to Figs. 8a and 8b, treating hydropower reservoirs as flood control reservoirs does not significantly impact the model simulated reservoir releases from most reservoirs, which partly supports the lack of differentiation between hydropower and flood control reservoirs in previous studies. However, the simulated reservoir storages are significantly different for ~ 44 % of the 296 reservoirs in terms of magnitude (NRMSE > 0.25) (Fig. 8b) and ~90% in terms of timing ($R^2< 0.5$) (Fig. 8a). Treating hydropower as flood control reservoirs thus has much more impact on the simulation of reservoir storage than releases, particularly in terms of timing. The NRMSE and R^2 values in Fig. 8 do not appear to relate to the reservoir sizes (figure not shown).

To explore the dynamics responsible for these broad patterns in Fig. 8, we select the Yenisey basin here to study in more detail. Here, the Yenisey basin is selected for demonstration because it has a mix of only flood control and hydropower reservoirs having just six reservoirs upstream of the GRDC site. In the Yenisey basin, the upstream area of the GRDC station is dominated by hydropower reservoirs, i.e., four hydropower reservoirs and two flood-control, as shown in supplementary Fig. S5a. Note that one of the two flood control reservoirs is located downstream of the hydropower reservoirs (Fig. S5a). This spatial arrangement allows us to evaluate the effects of simulating hydropower reservoirs as flood control reservoirs without interference from the third purpose (i.e., in cases where an irrigation reservoir is located downstream of a hydropower reservoir). Figure S5b (supplementary) shows the total simulated storage (sum of all six reservoirs) from *Xanthos-enhanced-sim2* and *Xanthos-enhanced-sim*. The difference in the magnitude of total simulated storage between the two simulations is very significant (KGE between them is 0.44). In *Xanthos-enhanced-sim2,* where all reservoirs are simulated as flood-control, the storage is relatively more variable from month to month, while *Xanthos-enhanced-sim* changes are more smooth, likely because the release aims to maintain mean annual flow in *Xanthos-enhanced-sim2*, which leads to releases that exceed inflow during the drier seasons and quick fill-up during the wet seasons. The streamflow comparison at the GRDC site (supplementary Fig. S5c) indicates that the difference in the simulated reservoir releases is also significant. The KGE values drop from 0.366 to 0.152 during the calibration period (1971-1980) and from 0.293 to 0.008 during the validation period (1981-1990) when simulating the hydropower reservoirs as flood control.

For those basins where hydropower reservoirs serve a secondary purpose compared to irrigation, flood control, or other types of reservoirs, there is no significant difference in the KGE values between *Xanthos-enhanced-sim2* and *Xanthos-enhanced-sim*, suggesting that treating hydropower reservoirs as flood control reservoirs do not lead to a significant difference in streamflow simulations at the regional/basin level. Figure 9 depicts the RII of the hydropower reservoirs on flow at GRDC stations for basins with one or more hydropower reservoirs (i.e., 51 of the 91 basins). The RII, shown here, corresponds to a hydropower reservoir with the largest storage within the basin. Figure 9 also shows a time series plot of the relative difference between *Xanthos-enhanced-sim2* and *Xanthos-enhanced-sim* storage and release for ten basins with relatively higher RII within different geographic regions.

The time series plots in Fig. 9 show the Storage Relative Difference (S-RD) and Release Relative Difference (R-RD) between the two scenarios. S-RD represents *Xanthos-enhanced-sim* storage minus *Xanthos-enhanced-sim2* storage scaled by the mean of the two storages. Similarly, R-RD is the scaled difference of simulated releases. From the time series plots of S-RD, one can see that, in some example basins, S-RD is > 0 (Fig. 9). This characteristic implies that when a reservoir is simulated as a hydropower reservoir, it generally maintains high storage with less variation than when simulated as a flood control reservoir. This can be attributed to our release policy for hydropower simulation, which targets maximum long-term revenue, where reservoir storage level is an essential component. Out of the 296 reservoirs, about 150 of them demonstrate this type of behavior for at least 50 % of the study period (1981-1990).

Flow downstream of hydropower reservoirs is also influenced by the change of reservoir purpose from hydropower to flood control (supplementary Fig. S5c). Similarly, a comparison of simulated releases (supplementary Fig. S6) shows the

difference between the simulated monthly releases in the peak and low flow periods. On the one hand, the release from the flood control reservoirs is high during peak flow periods because they aim to create excess storage capacity to attenuate inflow during the next flood event. On the other hand, the release from the hydropower reservoirs can only go up to the maximum turbine flow plus spillover. The Hanasaki et al. (2006) approach readjusts the mean annual flow depending on the reservoir's degree of regulation (i.e., capacity ratio to mean annual inflow). Therefore, in Xanthos, given that the readjusted mean annual flow is greater than the environmental flow (10% of the mean annual flow), release remains constant during the low flow periods. For hydropower reservoirs, low-flow releases are determined by a release policy intended to maximize revenue. Because of the changes in reservoir purpose, downstream reservoir releases are also modified.

Taken together, Figs. 7-9 and supplementary Figs. S4-S6 suggests that individual hydropower and flood control reservoirs behave very differently under the same climate and upstream conditions, particularly in terms of the simulated reservoir storage variations. Regarding regional-scale simulations, treating hydropower reservoirs as flood control leads to noticeably different simulated streamflow only in the basins where hydropower reservoirs dominate over the other types of reservoirs. For instance, for the Lower Colorado (RII=1.92), Caspian Sea South West Coast (RII=1.2), Yenisey (RII=1.02), Hudson Bay Coast (RII=1.32), and Sao Francisco (RII=0.67) basins, KGE improvement was >0.1 over the calibration period. The indicated RII corresponds to the total effect of hydropower reservoirs located upstream of the basin's GRDC site. This observation will have critical implications in studies where freshwater storage is the core interest since reservoir storage is a critical component of terrestrial freshwater storage. For instance, the number of hydropower reservoirs in many global basins is rapidly increasing (Zarfl et al., 2015). Hence, the potential of simulating them in GHMs is vital, as many of these basins' water use characteristics with hydropower reservoirs could change in the next decade or two if hundreds of new dams are built. Further, the observed distinct characteristics between hydropower and flood control reservoir storages have substantial implications for reservoir sedimentation, which is another essential feature the GHMs are increasingly looking to capture.

The results in this paper highlight some promising potential outcomes from accounting explicitly for hydropower objectives and operational behavior in GHMs. However, we note that it is premature to conclude from the above analysis that treating hydropower reservoirs as flood control leads to poor hydrological simulations and vice versa. Many reservoirs, particularly large ones, serve multiple purposes, so their behavior is controlled by multiple factors. This study takes the same simplification strategy adopted by all existing GHMs, i.e., treating each reservoir as having a single purpose. Overcoming this simplification in a GHM setting is beyond the scope of this study and is left for the future.

4 Discussion and Conclusions

This study adds a new water management module into the Xanthos model to improve its representation of global hydrological systems. The new water management module enhances Xanthos mainly by introducing reservoir regulation and local surface water withdrawal. We represent unique reservoir operation behavior for each reservoir based on its primary purpose, which can fall into the following three categories: irrigation, hydropower, and flood-control and others. In particular, hydropower

reservoirs have been treated as flood control reservoirs in previous GHM studies, whilst here we determined the operation rules for hydropower reservoirs via optimization that maximizes long-term hydropower production. We apply the enhanced Xanthos (*Xanthos-enhanced*) globally at a 0.5-degree spatial resolution and monthly time step. Validation against observed streamflow in 91 river gauge stations demonstrates improved performance over the original Xanthos (*Xanthos-original*) version. At the individual reservoir level, we show that hydropower and flood control reservoirs indeed behave quite differently, particularly in terms of reservoir storage variations. At the regional level, we show that treating hydropower reservoirs as flood control reservoirs leads to a noticeable impact on the simulated streamflow only in the basins where hydropower reservoirs are dominant. The model's performance improved by more than the KGE of 0.1 for some of the basins with significant Reservoir Impact Index (RII)(e.g., the Lower Colorado basin, the Caspian Sea South West Coast basin, Yenisey basin, the Hudson Bay Coast). The RII value corresponds to the total effect of hydropower reservoirs located upstream of a basin's GRDC site. Adding this new hydropower reservoir module can improve the analysis of finer-scale energy-water-land dynamics within frameworks capable of ingesting Xanthos outputs to capture water sector supply-demand dynamics (e.g., Graham et al., 2020; Khan et al., 2020; Birnbaum et al., 2022; Wild et al., 2021c, b). The benefits of distinguishing the unique behavior of hydropower reservoirs in GHMs may become more prominent if hydropower expansion in the coming decades occurs as planned (Zarfl et al., 2015).

There are several opportunities to improve *Xanthos-enhanced* further. First, in this study, we only determine optimal parameters for *Xanthos-enhanced* in 91 out of 235 large river basins globally due to the availability of observed streamflow data, and we assume each set of basin parameter values is uniform across grid cells within a basin. For future global applications of *Xanthos-enhanced*, one candidate approach to estimate the parameter values in the remaining river basins is to simply use average parameter values from the 91 basins that are gauged. Another possible approach is to estimate the parameters over these ungauged basins by invoking a hydrologic parameter regionalization strategy, i.e., estimating the parameter values *a priori* from existing climatology and landscape data based on multivariable regression techniques (Ye et al., 2014) or machine-learning methods (Abeshu et al., 2022). Second, the groundwater storage (both above and below confined aquifers) could be represented more explicitly in line with advancements in the representation of groundwater made by other GHMs (Gleeson et al., 2021), which will enable a more realistic representation of water supply with groundwater pumping as an additional source and potentially better streamflow simulation. Third, natural lakes should be represented in the model in addition to reservoirs. Lakes are an essential source of water supply, although they are not as heavily managed as reservoirs. They also have important impacts on the regional climate through their water and energy exchanges with the atmosphere. Fourth, hydrologically small reservoirs (i.e., those with a storage capacity less than 0.1 km^3) (Lehner et al., 2011) are currently not accounted for due to data limitations, but they potentially play an important role in the regional and global water supply. Last but not least, the representation of reservoirs could be enhanced by accounting for reservoir sedimentation, given that reservoir storage is being lost globally at a rate of 0.5% per year (Mahmood, 1987; White, 2001). Relatively simple, empirically-based approaches to capture these dynamics for reservoirs globally have been shown to be effective and can be borrowed from other open-source modeling frameworks (e.g., Wild et al., 2021a).

While our current two-stage calibration framework provides substantial insights, we anticipate its evolution towards a more comprehensive multi-gauge calibration approach. The existing framework, which relies on a single gauge per basin (typically the most downstream one), could potentially be expanded to multi-gauge calibration. Theoretically, this process would calibrate the model parameters using multiple gauges scattered throughout the basin, accommodating the spatial variability inherent in these parameters. Such an expansion could incorporate hierarchical and multi-objective optimization methods into the present two-stage framework. The hierarchical approach initiates calibration with the smaller, upstream sub-basins. The parameters determined at these stages subsequently inform the calibration of the larger, downstream basins, continuing in this fashion until the calibration of the most downstream gauge. This method capitalizes on the detailed information accessible at smaller scales, thereby assuring the consistency of large scale simulations with those on smaller scales. Incorporating multi-objective optimization, with objectives set at multiple gauges, is another approach that could augment the fidelity of the simulation within the two-stage calibration framework. This approach could mitigate discrepancies between simulated and observed discharges at multiple gauges simultaneously. Consequently, the model could represent a comprehensive array of hydrological behaviors across space, especially in large and heterogeneous basins where significant spatial variability in hydrological processes is common.

Even with the above limitations, the water management module we introduce here offers a more realistic representation of river systems in global hydrological models like Xanthos. The model has the potential to provide insight into the competition between changes in water availability (primarily affected by climate variability) and water demand (controlled mainly by human activities) at regional or global scales and support scientific analysis and planning in a complex socio-economic system setting under various future climate change and management scenarios.

Code availability

The current version of the model source code is available at https://github.com/gutabeshu/xanthos-wm, and steps for reproducing the model results and figures in the manuscript is available at https://github.com/gutabeshu/Abeshu-etal_2023_GMD.

Data availability

The supporting input data required to conduct the experiment is available at https://doi.org/10.5281/zenodo.7557403. The model output data for reproducing the figures in this paper is also available at https://doi.org/10.5281/zenodo.7557380

Author contribution

GWA developed the code, carried out the simulations, prepared the figures, and wrote the manuscript draft. GWA, HYL, MH, TW, ST, and MZ contributed to the methodology. GWA, HYL, TW, and MZ performed the analysis. All the authors contributed to the writing and discussion.

Acknowledgment

This research was supported by the U.S. Department of Energy, Office of Science, through the MultiSector Dynamics, Earth and Environmental System Modeling Program. G. Abeshu and H.-Y. Li also acknowledge the support from the U.S. National Science Foundation (EAR #1804560) and the Research Computing Data Core at the University of Houston for assistance with the computations carried out in this work. PNNL is operated for DOE by Battelle Memorial Institute under contract DE-AC05-76RL01830. The source code and input data for Xanthos used in this study can be freely downloaded at https://github.com/JGCRI/xanthos.

References

Abeshu, G. W., Li, H.-Y., Zhu, Z., Tan, Z., and Leung, L. R.: Median bed-material sediment particle size across rivers in the contiguous US, Earth Syst. Sci. Data, 14, 929–942, https://doi.org/10.5194/essd-14-929-2022, 2022.

Arango-Aramburo, S., Turner, S. W. D., Daenzer, K., Ríos-Ocampo, J. P., Hejazi, M. I., Kober, T., Álvarez-Espinosa, A. C., Romero-Otalora, G. D., and van der Zwaan, B.: Climate impacts on hydropower in Colombia: A multi-model assessment of power sector adaptation pathways, Energy Policy, 128, 179–188, https://doi.org/10.1016/j.enpol.2018.12.057, 2019.

Belletti, B., Garcia de Leaniz, C., Jones, J., Bizzi, S., Börger, L., Segura, G., Castelletti, A., van de Bund, W., Aarestrup, K., Barry, J., Belka, K., Berkhuysen, A., Birnie-Gauvin, K., Bussettini, M., Carolli, M., Consuegra, S., Dopico, E., Feierfeil, T., Fernández, S., Fernandez Garrido, P., Garcia-Vazquez, E., Garrido, S., Giannico, G., Gough, P., Jepsen, N., Jones, P. E., Kemp, P., Kerr, J., King, J., Łapińska, M., Lázaro, G., Lucas, M. C., Marcello, L., Martin, P., McGinnity, P., O'Hanley, J., Olivo del Amo, R., Parasiewicz, P., Pusch, M., Rincon, G., Rodriguez, C., Royte, J., Schneider, C. T., Tummers, J. S., Vallesi, S., Vowles, A., Verspoor, E., Wanningen, H., Wantzen, K. M., Wildman, L., and Zalewski, M.: More than one million barriers fragment Europe's rivers, Nature, 588, 436–441, https://doi.org/10.1038/s41586-020-3005-2, 2020.

Best, M. J., Pryor, M., Clark, D. B., Rooney, G. G., Essery, R. . L. H., Ménard, C. B., Edwards, J. M., Hendry, M. A., Porson, A., Gedney, N., Mercado, L. M., Sitch, S., Blyth, E., Boucher, O., Cox, P. M., Grimmond, C. S. B., and Harding, R. J.: The Joint UK Land Environment Simulator (JULES), model description – Part 1: Energy and water fluxes, Geosci. Model Dev., 4, 677–699, https://doi.org/10.5194/gmd-4-677-2011, 2011.

Beven, K.: A manifesto for the equifinality thesis, J. Hydrol., 320, 18–36, https://doi.org/10.1016/j.jhydrol.2005.07.007, 2006.

Beven, K.: Parameter Estimation and Predictive Uncertainty, in: Rainfall-Runoff Modelling, Wiley, 231–287, https://doi.org/10.1002/9781119951001.ch7, 2012.

Biemans, H., Haddeland, I., Kabat, P., Ludwig, F., Hutjes, R. W. A., Heinke, J., Von Bloh, W., and Gerten, D.: Impact of reservoirs on river discharge and irrigation water supply during the 20th century, Water Resour. Res., 47, 1–15, https://doi.org/10.1029/2009WR008929, 2011.

Birnbaum, A., Lamontagne, J., Wild, T., Dolan, F., and Yarlagadda, B.: Drivers of Future Physical Water Scarcity and Its Economic Impacts in Latin America and the Caribbean, Earth's Futur., 10, 1–21, https://doi.org/10.1029/2022EF002764, 2022.

Boulange, J., Hanasaki, N., Yamazaki, D., and Pokhrel, Y.: Role of dams in reducing global flood exposure under climate change, Nat. Commun., 12, 1–7, https://doi.org/10.1038/s41467-020-20704-0, 2021.

Branstetter, M. L. and Erickson, D. J.: Continental runoff dynamics in the Community Climate System Model 2 (CCSM2) control simulation, J. Geophys. Res. Atmos., 108, 1–17, https://doi.org/10.1029/2002jd003212, 2003.

Burek, P., Satoh, Y., Kahil, T., Tang, T., Greve, P., Smilovic, M., Guillaumot, L., Zhao, F., and Wada, Y.: Development of the Community Water Model (CWatM v1.04) - A high-resolution hydrological model for global and regional assessment of integrated water resources management, Geosci. Model Dev., 13, 3267–3298, https://doi.org/10.5194/gmd-13-3267-2020,

2020.

Calvin, K., Patel, P., Clarke, L., Asrar, G., Bond-Lamberty, B., Yiyun Cui, R., Di Vittorio, A., Dorheim, K., Edmonds, J., Hartin, C., Hejazi, M., Horowitz, R., Iyer, G., Kyle, P., Kim, S., Link, R., Mcjeon, H., Smith, S. J., Snyder, A., Waldhoff, S., and Wise, M.: GCAM v5.1: Representing the linkages between energy, water, land, climate, and economic systems, Geosci. Model Dev., 12, 677–698, https://doi.org/10.5194/gmd-12-677-2019, 2019.

D. N. Moriasi, J. G. Arnold, M. W. Van Liew, R. L. Bingner, R. D. Harmel, and T. L. Veith: Model Evaluation Guidelines for Systematic Quantification of Accuracy in Watershed Simulations, Trans. ASABE, 50, 885–900, https://doi.org/10.13031/2013.23153, 2007.

Döll, P., Fiedler, K., and Zhang, J.: Global-scale analysis of river flow alterations due to water withdrawals and reservoirs, Hydrol. Earth Syst. Sci., 13, 2413–2432, https://doi.org/10.5194/hess-13-2413-2009, 2009.

Gleeson, T., Wagener, T., Döll, P., Zipper, S. C., West, C., Wada, Y., Taylor, R., Scanlon, B., Rosolem, R., Rahman, S., Oshinlaja, N., Maxwell, R., Lo, M. H., Kim, H., Hill, M., Hartmann, A., Fogg, G., Famiglietti, J. S., Ducharne, A., De Graaf, I., Cuthbert, M., Condon, L., Bresciani, E., and Bierkens, M. F. P.: GMD perspective: The quest to improve the evaluation of groundwater representation in continental-to global-scale models, Geosci. Model Dev., 14, 7545–7571, https://doi.org/10.5194/gmd-14-7545-2021, 2021.

Graham, N. T., Hejazi, M. I., Chen, M., Davies, E. G. R., Edmonds, J. A., Kim, S. H., Turner, S. W. D., Li, X., Vernon, C. R., Calvin, K., Miralles-Wilhelm, F., Clarke, L., Kyle, P., Link, R., Patel, P., Snyder, A. C., and Wise, M. A.: Humans drive future water scarcity changes across all Shared Socioeconomic Pathways, Environ. Res. Lett., 15, https://doi.org/10.1088/1748-9326/ab639b, 2020.

Grill, G., Lehner, B., Thieme, M., Geenen, B., Tickner, D., Antonelli, F., Babu, S., Borrelli, P., Cheng, L., Crochetiere, H., Ehalt Macedo, H., Filgueiras, R., Goichot, M., Higgins, J., Hogan, Z., Lip, B., McClain, M. E., Meng, J., Mulligan, M., Nilsson, C., Olden, J. D., Opperman, J. J., Petry, P., Reidy Liermann, C., Sáenz, L., Salinas-Rodríguez, S., Schelle, P., Schmitt, R. J. P., Snider, J., Tan, F., Tockner, K., Valdujo, P. H., van Soesbergen, A., and Zarfl, C.: Mapping the world's free-flowing rivers, Nature, 569, 215–221, https://doi.org/10.1038/s41586-019-1111-9, 2019.

Grogan, D. S., Zuidema, S., Prusevich, A., Wollheim, W. M., Glidden, S., and Lammers, R. B.: WBM : A scalable gridded global hydrologic model with water tracking functionality, Geosci. Model Dev., 08, 1–54, 2022.

Gupta, H. V., Kling, H., Yilmaz, K. K., and Martinez, G. F.: Decomposition of the mean squared error and NSE performance criteria: Implications for improving hydrological modelling, J. Hydrol., 377, 80–91, https://doi.org/10.1016/j.jhydrol.2009.08.003, 2009.

Haddeland, I., Skaugen, T., and Lettenmaier, D. P.: Anthropogenic impacts on continental surface water fluxes, Geophys. Res. Lett., 33, 2–5, https://doi.org/10.1029/2006GL026047, 2006.

Hanasaki, N., Kanae, S., and Oki, T.: A reservoir operation scheme for global river routing models, J. Hydrol., 327, 22–41, https://doi.org/10.1016/j.jhydrol.2005.11.011, 2006.

Hanasaki, N., Kanae, S., Oki, T., Masuda, K., Motoya, K., Shirakawa, N., Shen, Y., and Tanaka, K.: An integrated model for

the assessment of global water resources - Part 1: Model description and input meteorological forcing, Hydrol. Earth Syst. Sci., 12, 1007–1025, https://doi.org/10.5194/hess-12-1007-2008, 2008.

Hejazi, M., Edmonds, J., Clarke, L., Hejazi, M. I., Edmonds, J., Clarke, L., Kyle, P., Davies, E., Chaturvedi, V., Eom, J., Wise, M., Patel, P., and Calvin, K.: Integrated assessment of global water scarcity over the 21st century-Part 2: Climate change mitigation policies Sustainable Development, Uncertainties, and India's Climate Policy: Pathways towards Nationally Determined Contribution and Mid-Century Strateg, Hydrol. Earth Syst. Sci. Discuss, 10, 3383–3425, https://doi.org/10.5194/hessd-10-3383-2013, 2013.

Hejazi, M. I., Edmonds, J., Clarke, L., Kyle, P., Davies, E., Chaturvedi, V., Wise, M., Patel, P., Eom, J., and Calvin, K.: Integrated assessment of global water scarcity over the 21st century under multiple climate change mitigation policies, Hydrol. Earth Syst. Sci., 18, 2859–2883, https://doi.org/10.5194/hess-18-2859-2014, 2014.

Hirpa, F. A., Salamon, P., Beck, H. E., Lorini, V., Alfieri, L., Zsoter, E., and Dadson, S. J.: Calibration of the Global Flood Awareness System (GloFAS) using daily streamflow data, J. Hydrol., 566, 595–606, https://doi.org/10.1016/j.jhydrol.2018.09.052, 2018.

Huang, Z., Hejazi, M., Li, X., Tang, Q., Vernon, C., Leng, G., Liu, Y., Döll, P., Eisner, S., Gerten, D., Hanasaki, N., and Wada, Y.: Global gridded monthly sectoral water use dataset for 1971-2010: v2, https://doi.org/https://doi.org/https://doi.org/10.5281/zenodo.1209296, 2018a.

Huang, Z., Hejazi, M., Li, X., Tang, Q., Vernon, C., Leng, G., Liu, Y., Döll, P., Eisner, S., Gerten, D., Hanasaki, N., and Wada, Y.: Reconstruction of global gridded monthly sectoral water withdrawals for 1971-2010 and analysis of their spatiotemporal patterns, Hydrol. Earth Syst. Sci., 22, 2117–2133, https://doi.org/10.5194/hess-22-2117-2018, 2018b.

Khan, Z., Wild, T. B., Silva Carrazzone, M. E., Gaudioso, R., Mascari, M. P., Bianchi, F., Weinstein, F., Pérez, F., Pérez, W., Miralles-Wilhelm, F., Clarke, L., Hejazi, M., Vernon, C. R., Kyle, P., Edmonds, J., and Muoz Castillo, R.: Integrated energy-water-land nexus planning to guide national policy: An example from Uruguay, Environ. Res. Lett., 15, https://doi.org/10.1088/1748-9326/ab9389, 2020.

van der Knijff, J. M., Younis, J., and de Roo, A. P. J.: LISFLOOD: A GIS-based distributed model for river basin scale water balance and flood simulation, Int. J. Geogr. Inf. Sci., 24, 189–212, https://doi.org/10.1080/13658810802549154, 2010.

Knoben, W. J. M., Freer, J. E., and Woods, R. A.: Technical note: Inherent benchmark or not? Comparing Nash-Sutcliffe and Kling-Gupta efficiency scores, Hydrol. Earth Syst. Sci., 23, 4323–4331, https://doi.org/10.5194/hess-23-4323-2019, 2019.

Lehner, B., Liermann, C. R., Revenga, C., Vörömsmarty, C., Fekete, B., Crouzet, P., Döll, P., Endejan, M., Frenken, K., Magome, J., Nilsson, C., Robertson, J. C., Rödel, R., Sindorf, N., and Wisser, D.: High-resolution mapping of the world's reservoirs and dams for sustainable river-flow management, Front. Ecol. Environ., 9, 494–502, https://doi.org/10.1890/100125, 2011.

Li, H., Huang, M., Wigmosta, M. S., Ke, Y., Coleman, A. M., Leung, L. R., Wang, A., and Ricciuto, D. M.: Evaluating runoff simulations from the Community Land Model 4.0 using observations from flux towers and a mountainous watershed, J. Geophys. Res. Atmos., 116, https://doi.org/10.1029/2011JD016276, 2011.

Li, H., Abeshu, G., Zhu, Z., Tan, Z., and Leung, L. R.: A national map of riverine median bed-material particle size over CONUS(1.1) [Data set], https://doi.org/https://doi.org/10.5281/zenodo.4921987, 2021.

Li, H. Y., Leung, L. R., Getirana, A., Huang, M., Wu, H., Xu, Y., Guo, J., and Voisin, N.: Evaluating global streamflow simulations by a physically based routing model coupled with the community land model, J. Hydrometeorol., 16, 948–971, https://doi.org/10.1175/JHM-D-14-0079.1, 2015.

Li, X., Vernon, C. R., Hejazi, M. I., Link, R. P., Feng, L., Liu, Y., and Rauchenstein, L. T.: Xanthos – A Global Hydrologic Model, J. Open Res. Softw., 5, 21, https://doi.org/10.5334/jors.181, 2017.

Liu, Y., Hejazi, M., Li, H., Zhang, X., and Leng, G.: A hydrological emulator for global applications-HE v1.0.0, Geosci. Model Dev., 11, 1077–1092, https://doi.org/10.5194/gmd-11-1077-2018, 2018.

López, J. and Francés, F.: Non-stationary flood frequency analysis in continental Spanish rivers, using climate and reservoir indices as external covariates, Hydrol. Earth Syst. Sci., 17, 3189–3203, https://doi.org/10.5194/hess-17-3189-2013, 2013.

Loucks, D. P., Beek, E. van, Stedinger, J. R., Dijkman, J. P. M., and Villars, M. T.: Water resource systems planning and management: An introduction to methods, models, and applications, Springer International Publishing, Cham, 1–624 pp., https://doi.org/10.1007/978-3-319-44234-1, 2017.

Mahmood, K.: Reservoir sedimentation: impact, extent, and mitigation, Technical Report, International Bank for Reconstruction and Development, Washington, DC (USA), 1987.

Martinez, G. F. and Gupta, H. V.: Toward improved identification of hydrological models: A diagnostic evaluation of the "abcd" monthly water balance model for the conterminous United States, Water Resour. Res., 46, 1–21, https://doi.org/10.1029/2009WR008294, 2010.

Martinez, G. F. and Gupta, H. V.: Hydrologic consistency as a basis for assessing complexity of monthly water balance models for the continental United States, Water Resour. Res., 47, 1–18, https://doi.org/10.1029/2011WR011229, 2011.

McKay, M. D., Beckman, R. J., and Conover, W. J.: Comparison of Three Methods for Selecting Values of Input Variables in the Analysis of Output from a Computer Code, Technometrics, 21, 239–245, https://doi.org/10.1080/00401706.1979.10489755, 1979.

Moges, E., Demissie, Y., Larsen, L., and Yassin, F.: Review: Sources of hydrological model uncertainties and advances in their analysis, Water (Switzerland), 13, 1–23, https://doi.org/10.3390/w13010028, 2021.

Müller Schmied, H., Caceres, D., Eisner, S., Flörke, M., Herbert, C., Niemann, C., Asali Peiris, T., Popat, E., Theodor Portmann, F., Reinecke, R., Schumacher, M., Shadkam, S., Telteu, C. E., Trautmann, T., and Döll, P.: The global water resources and use model WaterGAP v2.2d: Model description and evaluation, Geosci. Model Dev., 14, 1037–1079, https://doi.org/10.5194/gmd-14-1037-2021, 2021.

Piccardi, C. and Soncini-Sessa, R.: Stochastic dynamic programming for reservoir optimal control: Dense discretization and inflow correlation assumption made possible by parallel computing, Water Resour. Res., 27, 729–741, https://doi.org/10.1029/90WR02766, 1991.

Pokhrel, Y., Hanasaki, N., Koirala, S., Cho, J., Yeh, P. J. F., Kim, H., Kanae, S., and Oki, T.: Incorporating anthropogenic

water regulation modules into a land surface model, J. Hydrometeorol., 13, 255–269, https://doi.org/10.1175/JHM-D-11-013.1, 2012.

Pokhrel, Y. N., Koirala, S., Yeh, P. J.-F., Hanasaki, N., Longuevergne, L., Kanae, S., and Oki, T.: Incorporation of groundwater pumping in a global Land Surface Model with the representation of human impacts, Water Resour. Res., 51, 78–96, https://doi.org/10.1002/2014WR015602, 2015.

De Roo, A. P. J., Wesseling, C. G., and Van Deursen, W. P. A.: Physically based river basin modelling within a GIS: The LISFLOOD model, Hydrol. Process., 14, 1981–1992, https://doi.org/10.1002/1099-1085(20000815/30)14:11/12<1981::aid-hyp49>3.0.co;2-f, 2000.

Santos da Silva, S. R., Hejazi, M. I., Iyer, G., Wild, T. B., Binsted, M., Miralles-Wilhelm, F., Patel, P., Snyder, A. C., and Vernon, C. R.: Power sector investment implications of climate impacts on renewable resources in Latin America and the Caribbean, Nat. Commun., 12, 1–12, https://doi.org/10.1038/s41467-021-21502-y, 2021.

Schaphoff, S., Von Bloh, W., Rammig, A., Thonicke, K., Biemans, H., Forkel, M., Gerten, D., Heinke, J., Jägermeyr, J., Knauer, J., Langerwisch, F., Lucht, W., Müller, C., Rolinski, S., and Waha, K.: LPJmL4 - A dynamic global vegetation model with managed land - Part 1: Model description, Geosci. Model Dev., 11, 1343–1375, https://doi.org/10.5194/gmd-11-1343-2018, 2018.

Schmied, M. H., Cáceres, D., Eisner, S., Flörke, M., Herbert, C., Niemann, C., Peiris, T. A., Popat, E., Portmann, F. T., Reinecke, R., Schumacher, M., Shadkam, S., Telteu, C.-E., Trautmann, T., and Döll, P.: The global water resources and use model WaterGAP v2.2d: model description and evaluation, Geosci. Model Dev., 14, 1037–1079, https://doi.org/10.5194/gmd-14-1037-2021, 2021.

Shen, Y., Ruijsch, J., Lu, M., Sutanudjaja, E. H., and Karssenberg, D.: Random forests-based error-correction of streamflow from a large-scale hydrological model: Using model state variables to estimate error terms, Comput. Geosci., 159, 105019, https://doi.org/10.1016/j.cageo.2021.105019, 2022.

Sutanudjaja, E. H., Van Beek, R., Wanders, N., Wada, Y., Bosmans, J. H. C., Drost, N., Van Der Ent, R. J., De Graaf, I. E. M., Hoch, J. M., De Jong, K., Karssenberg, D., López López, P., Peßenteiner, S., Schmitz, O., Straatsma, M. W., Vannametee, E., Wisser, D., and Bierkens, M. F. P.: PCR-GLOBWB 2: A 5 arcmin global hydrological and water resources model, Geosci. Model Dev., 11, 2429–2453, https://doi.org/10.5194/gmd-11-2429-2018, 2018.

Telteu, C. E., Müller Schmied, H., Thiery, W., Leng, G., Burek, P., Liu, X., Boulange, J. E. S., Andersen, L. S., Grillakis, M., Gosling, S. N., Satoh, Y., Rakovec, O., Stacke, T., Chang, J., Wanders, N., Shah, H. L., Trautmann, T., Mao, G., Hanasaki, N., Koutroulis, A., Pokhrel, Y., Samaniego, L., Wada, Y., Mishra, V., Liu, J., Döll, P., Zhao, F., Gädeke, A., Rabin, S. S., and Herz, F.: Understanding each other's models An introduction and a standard representation of 16 global water models to support intercomparison, improvement, and communication, Geosci. Model Dev., 14, 3843–3878, https://doi.org/10.5194/gmd-14-3843-2021, 2021.

Tennant, D. L.: Instream Flow Regimens for Fish, Wildlife, Recreation and Related Environmental Resources, Fisheries, 1, 6–10, https://doi.org/10.1577/1548-8446(1976)001<0006:IFRFFW>2.0.CO;2, 1976.

Thomas, H. A.: Improved Methods for National tvater Assessment, U.S. Geol. Surv. Water Resour., 44, 1981.

Turner, S. W. D.: Reservoir (Tools for Analysis, Design, and Operation of Water Supply Storages), https://doi.org/https://geomodeling.njnu.edu.cn/modelItem/074783d2-6218-4b9d-b1e2-d93132d3b030, 2016.

Turner, S. W. D., Ng, J. Y., and Galelli, S.: Examining global electricity supply vulnerability to climate change using a high-fidelity hydropower dam model, Sci. Total Environ., 590–591, 663–675, https://doi.org/10.1016/j.scitotenv.2017.03.022, 2017.

Vernon, C. R., Hejazi, M. I., Turner, S. W. D., Liu, Y., Braun, C. J., Li, X., and Link, R. P.: A global hydrologic framework to accelerate scientific discovery, J. Open Res. Softw., 7, 1–7, https://doi.org/10.5334/jors.245, 2019.

Voisin, N., Li, H., Ward, D., Huang, M., Wigmosta, M., and Leung, L. R.: On an improved sub-regional water resources management representation for integration into earth system models, Hydrol. Earth Syst. Sci., 17, 3605–3622, https://doi.org/10.5194/hess-17-3605-2013, 2013.

Votruba, L. and Broza, V.: Flood-control Function of Reservoirs, in: Water Management in Reservoirs, 295–296, https://doi.org/10.1016/S0167-5648(08)70640-3, 1989.

Walsh, R. P. D. and Lawler, D. M.: Rainfall seasonality: Description, spatial patterns and change through time, Weather, 36, 201–208, https://doi.org/10.1002/j.1477-8696.1981.tb05400.x, 1981.

Wan, W., Zhao, J., Li, H. Y., Mishra, A., Ruby Leung, L., Hejazi, M., Wang, W., Lu, H., Deng, Z., Demissisie, Y., and Wang, H.: Hydrological Drought in the Anthropocene: Impacts of Local Water Extraction and Reservoir Regulation in the U.S, J. Geophys. Res. Atmos., 122, 11,313-11,328, https://doi.org/10.1002/2017JD026899, 2017.

Wan, W., Zhao, J., Li, H. Y., Mishra, A., Hejazi, M., Lu, H., Demissie, Y., and Wang, H.: A Holistic View of Water Management Impacts on Future Droughts: A Global Multimodel Analysis, J. Geophys. Res. Atmos., 123, 5947–5972, https://doi.org/10.1029/2017JD027825, 2018.

Wang, W., Li, H. Y., Leung, L. R., Yigzaw, W., Zhao, J., Lu, H., Deng, Z., Demisie, Y., and Blöschl, G.: Nonlinear Filtering Effects of Reservoirs on Flood Frequency Curves at the Regional Scale, Water Resour. Res., 53, 8277–8292, https://doi.org/10.1002/2017WR020871, 2017.

Weedon, G. P., Gomes, S., Viterbo, P., Shuttleworth, W. J., Blyth, E., Österle, H., Adam, J. C., Bellouin, N., Boucher, O., and Best, M.: Creation of the WATCH Forcing Data and Its Use to Assess Global and Regional Reference Crop Evaporation over Land during the Twentieth Century, J. Hydrometeorol., 12, 823–848, https://doi.org/10.1175/2011JHM1369.1, 2011.

White, R.: Evacuation of sediments from reservoirs, Thomas Telford Publishing, https://doi.org/10.1680/eosfr.29538, 2001.

Wild, T. B., Birnbaum, A. N., Reed, P. M., and Loucks, D. P.: An open source reservoir and sediment simulation framework for identifying and evaluating siting, design, and operation alternatives, Environ. Model. Softw., 136, 104947, https://doi.org/10.1016/j.envsoft.2020.104947, 2021a.

Wild, T. B., Khan, Z., Clarke, L., Hejazi, M., Bereslawski, J. L., Suriano, M., Roberts, P., Casado, J., Miralles-Wilhelm, F., Gavino-Novillo, M., Muñoz-Castillo, R., Moreda, F., Zhao, M., Yarlagadda, B., Lamontagne, J., and Birnbaum, A.: Integrated energy-water-land nexus planning in the Colorado River Basin (Argentina), Reg. Environ. Chang., 21, 62,

https://doi.org/10.1007/s10113-021-01775-1, 2021b.

Wild, T. B., Khan, Z., Zhao, M., Suriano, M., Bereslawski, J. L., Roberts, P., Casado, J., Gaviño-Novillo, M., Clarke, L., Hejazi, M., Miralles-Wilhelm, F., Muñoz-Castillo, R., Vernon, C., Snyder, A., Yarlagadda, B., Birnbaum, A., Lamontagne, J., White, D., and Ojeda-Matos, G.: The Implications of Global Change for the Co-Evolution of Argentina's Integrated Energy-Water-Land Systems, Earth's Futur., 9, https://doi.org/10.1029/2020EF001970, 2021c.

Wisser, D., Fekete, B. M., Vörösmarty, C. J., and Schumann, A. H.: Reconstructing 20th century global hydrography: A contribution to the Global Terrestrial Network- Hydrology (GTN-H), Hydrol. Earth Syst. Sci., 14, 1–24, https://doi.org/10.5194/hess-14-1-2010, 2010.

Wu, H., Kimball, J. S., Mantua, N., and Stanford, J.: Automated upscaling of river networks for macroscale hydrological modeling, Water Resour. Res., 47, 1–18, https://doi.org/10.1029/2009WR008871, 2011.

Yassin, F., Razavi, S., Elshamy, M., Davison, B., Sapriza-Azuri, G., and Wheater, H.: Representation and improved parameterization of reservoir operation in hydrological and land-surface models, Hydrol. Earth Syst. Sci., 23, 3735–3764, https://doi.org/10.5194/hess-23-3735-2019, 2019.

Ye, S., Li, H. Y., Huang, M., Ali, M., Leng, G., Leung, L. R., Wang, S. wen, and Sivapalan, M.: Regionalization of subsurface stormflow parameters of hydrologic models: Derivation from regional analysis of streamflow recession curves, J. Hydrol., 519, 670–682, https://doi.org/10.1016/j.jhydrol.2014.07.017, 2014.

Yoshida, T., Hanasaki, N., Nishina, K., Boulange, J., Okada, M., and Troch, P. A.: Inference of Parameters for a Global Hydrological Model: Identifiability and Predictive Uncertainties of Climate-Based Parameters, Water Resour. Res., 58, https://doi.org/10.1029/2021WR030660, 2022.

Zeng, X., Hu, T., Cai, X., Zhou, Y., and Wang, X.: Improved dynamic programming for parallel reservoir system operation optimization, Adv. Water Resour., 131, https://doi.org/10.1016/j.advwatres.2019.07.003, 2019.

Zhang, X., Li, H.-Y., Deng, Z. D., Ringler, C., Gao, Y., Hejazi, M. I., and Leung, L. R.: Impacts of climate change, policy and Water-Energy-Food nexus on hydropower development, Renew. Energy, 116, 827–834, https://doi.org/10.1016/j.renene.2017.10.030, 2018.

Zhang, X., Li, H. Y., Deng, Z. D., Leung, L. R., Skalski, J. R., and Cooke, S. J.: On the variable effects of climate change on Pacific salmon, Ecol. Modell., 397, 95–106, https://doi.org/10.1016/j.ecolmodel.2019.02.002, 2019.

Zhang, X., Li, H. Y., Leung, L. R., Liu, L., Hejazi, M. I., Forman, B. A., and Yigzaw, W.: River Regulation Alleviates the Impacts of Climate Change on U.S. Thermoelectricity Production, J. Geophys. Res. Atmos., 125, https://doi.org/10.1029/2019JD031618, 2020.

Zhou, T., Leung, L. R., Leng, G., Voisin, N., Li, H. Y., Craig, A. P., Tesfa, T., and Mao, Y.: Global Irrigation Characteristics and Effects Simulated by Fully Coupled Land Surface, River, and Water Management Models in E3SM, J. Adv. Model. Earth Syst., 12, 1–18, https://doi.org/10.1029/2020MS002069, 2020.

Zhou, Y., Hejazi, M., Smith, S., Edmonds, J., Li, H., Clarke, L., Calvin, K., and Thomson, A.: A comprehensive view of global potential for hydro-generated electricity, Energy Environ. Sci., 8, 2622–2633, https://doi.org/10.1039/C5EE00888C, 2015.

905

Tables

Table 1: List of global hydrological models with reservoir representations. The *Domain* column indicates the spatial scale at which the model has been applied. The *Representations* column describes how each reservoir class (from the Reservoir classification column) is simulated. In all cases, the reservoirs are integrated into the models. The Reservoir Classification column shows how the reservoirs were represented.

Model	Domain	Reservoir Classification	Representations	Reference	websites
H08	Global	Irrigation/ Non-Irrigation	Irrigation: release is based on demand Non-Irrigation: treated as flood control, where releases are adjustments to the mean annual inflow based on storage	Hanasaki et al. (2008) Boulange et al. (2021) Yoshida et al. (2022)	http://h08.nies.go.jp/h08/index.html
WaterGAP	Global	Irrigation/ Non-Irrigation	Modified Hanasaki et al. (2006)	Döll et al. (2009) Müller Schmied et al. (2021)	www.watergap.de
WBMplus	Global	Irrigation/ Non-Irrigation	Modified Hanasaki et al. (2006)	Wisser et al. (2010) Grogan et al. (2022)	https://wsag.unh.edu/wbm.html
PCR-GLOBWB	Global	Irrigation/ Non-Irrigation	Uses a default strategy aimed at passing the average discharge while maintaining levels between a minimum and maximum storage. For irrigation, release based on downstream water demand is possible for an elaborate release strategy.	Sutanudjaja et al. (2018) Shen et al. (2022)	https://globalhydrology.nl/research/models/pcr-globwb-2-0/
LISFLOOD	Europe, Global	No classification based on the purpose	Uses a simple general reservoir operation scheme, simulated as an outflow function between three storage limits: minimum outflow, non-damaging outflow, and normal outflow	De Roo et al. (2000) van der Knijff et al. (2010) Hirpa et al. (2018)	https://ec-jrc.github.io/lisflood-model/3_03_optLISFLOOD_reservoirs/
MATSIRO	Global	Irrigation/ Non-Irrigation	Modified Hanasaki et al. (2006)	Pokhrel et al. (2012)	http://hydro.iis.u-tokyo.ac.jp/~

				Pokhrel et al. (2015) Telteu et al. (2021)	sujan/research/models/matsiro.html
LPJmL4	Global	Irrigation/ Non-Irrigation	Irrigation: assumed to release water proportionally to gross irrigation water demand. Other purposes (hydropower, flood control, etc.): assumed to be designed for releasing a constant volume throughout the year	Schaphoff et al. (2018) Telteu et al. (2021)	http://www.pik-potsdam.de/research/projects/activities/biosphere-water-modelling/lpjml
CWatM	Global	No classification based on the purpose	Adopts LISFLOOD generic reservoir operation method. Reservoirs are simulated as outflow functions between three storage limits (conservative, normal, flood) and three outflow functions (minimum, normal, non-damaging)	Burek et al. (2020)	https://cwatm.iiasa.ac.at/modeldesign.html
MOSART-WM	Global	Irrigation/ Flood control / Combination of both and others	The operating rules are determined based on historical long-term mean monthly inflow, reservoir characteristics, and reservoir purpose	Zhou et al. (2020)	https://im3.pnnl.gov/model?model=MOSART-WM

Table 2: **List of model parameters, description, and ranges. The parameters a, c, d, m, β, and α are dimensionless, and the unit for parameter b is meters. The value of α is fixed at 0.85 following Hanasaki et al. (2006).**

Parameter	Description	Range	Type
a	Propensity of runoff to occur before the soil is fully saturated	0–1	runoff
b	Upper limit on the sum of evapotranspiration and soil moisture storage	0–8	runoff
c	Degree of recharge to groundwater	0–1	runoff
d	Release rate of groundwater to baseflow	0–1	runoff
m	Snowmelt coefficient	0–1	runoff
β	Velocity adjustment coefficient	0–10	routing
α	Reservoir capacity reduction factor	0–1	reservoir

Table 3: Types of modeling experiments performed in this study

Scenario Name	Description
Xanthos-original-sim	Simulated flow is obtained by routing calibrated runoff data generated by Liu et al. (2018). No water management components (Vernon et al., 2019) are implemented. Routing is performed using the optimal velocity adjustment coefficient obtained after stage-2 parameter filtering.
Xanthos-enhanced-sim	Simulated result from *Xanthos-enhanced*. Simulated streamflow is obtained by routing runoff generated with optimal parameter sets determined following a new parameter determination strategy (described in Section 2.4). Water management components (i.e., reservoirs and water consumption) are included. Reservoirs are classified into hydropower, irrigation, and flood control category types. A unique operation scheme is applied for each reservoir type (Fig. 2).
Xanthos-enhanced-sim2	Similar to *Xanthos-enhanced-sim*, but reservoirs are classified into two types only: irrigation and flood control. All hydropower reservoirs are merged into the flood control category. Comparison to the *Xanthos-enhanced-sim* experiment reveals the value of representing hydropower as a unique class of reservoir behavior, a key contribution of this paper.

Figures

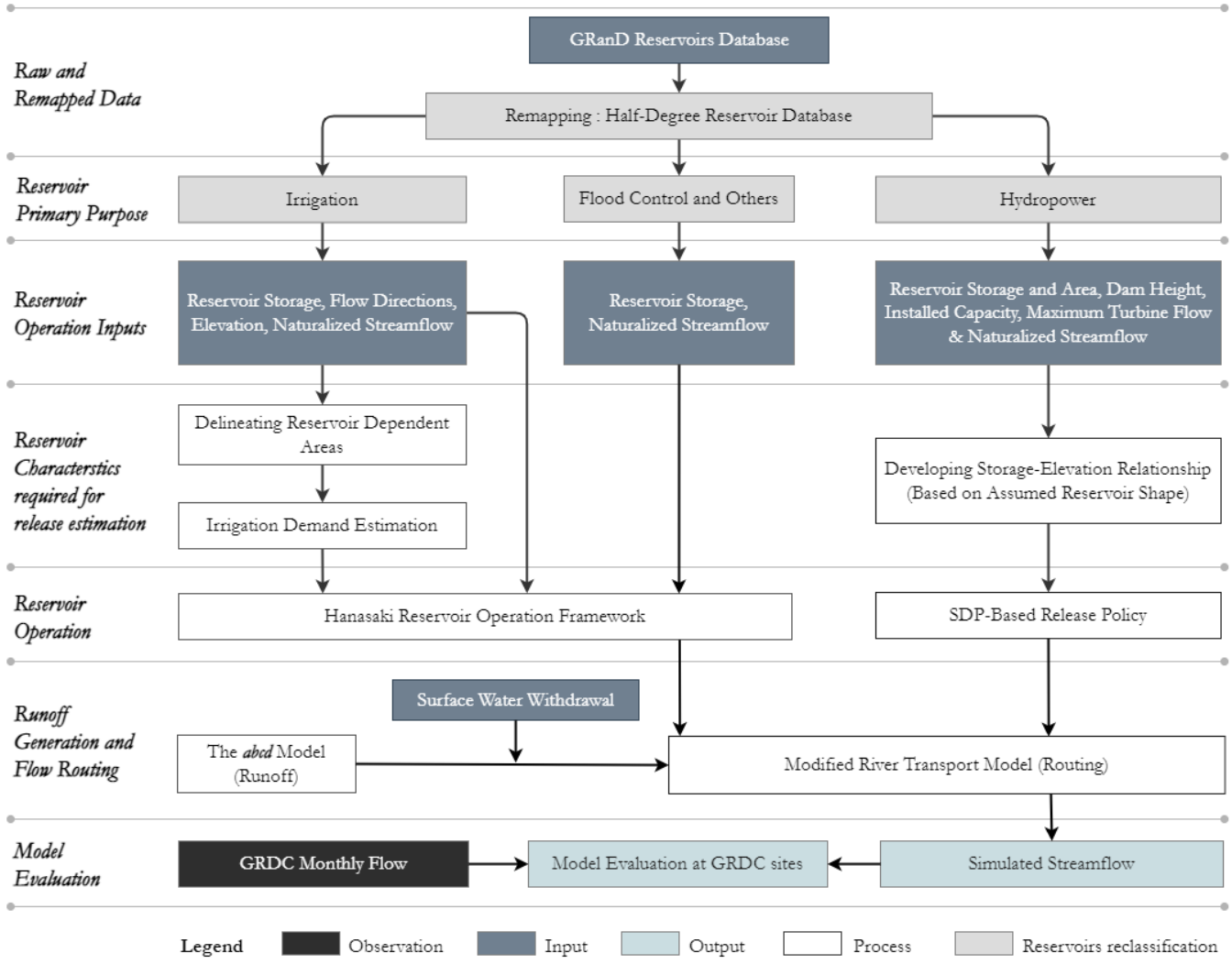

Figure 1: A detailed schematic of the river routing and reservoir management module in *Xanthos-enhanced*.

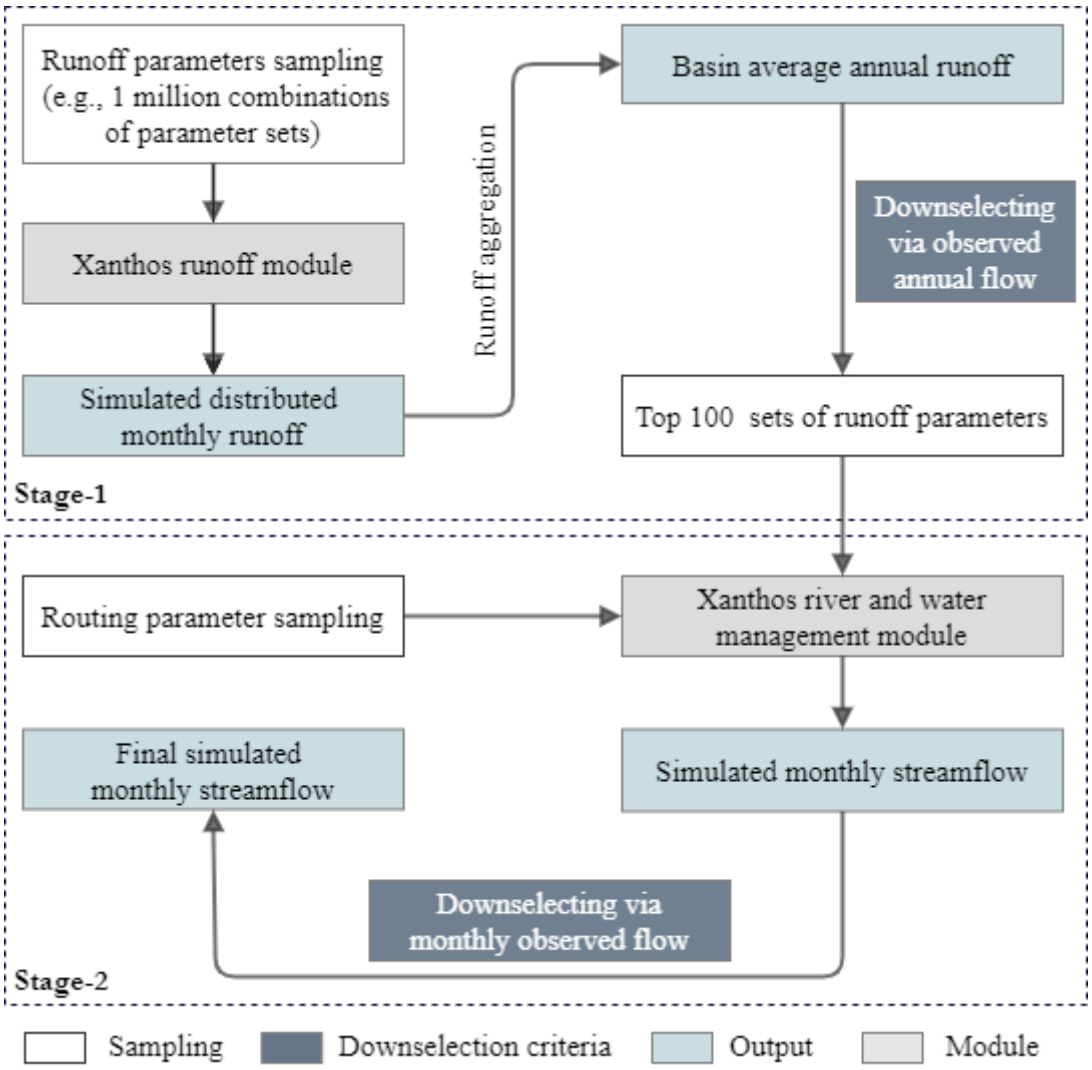

10 **Figure 2: Runoff and routing parameters selection strategy for *Xanthos-enhanced*. Each component of the process is categorized as one of the following: (1) sampling, wherein parameter combinations are sampled; (2) downselection criteria, which are applied to downsample a larger parameter set into a smaller, more favorable subset; (3) outputs, which describes model outputs; and (4) modules, which describes Xanthos model methods (or sections of code).**

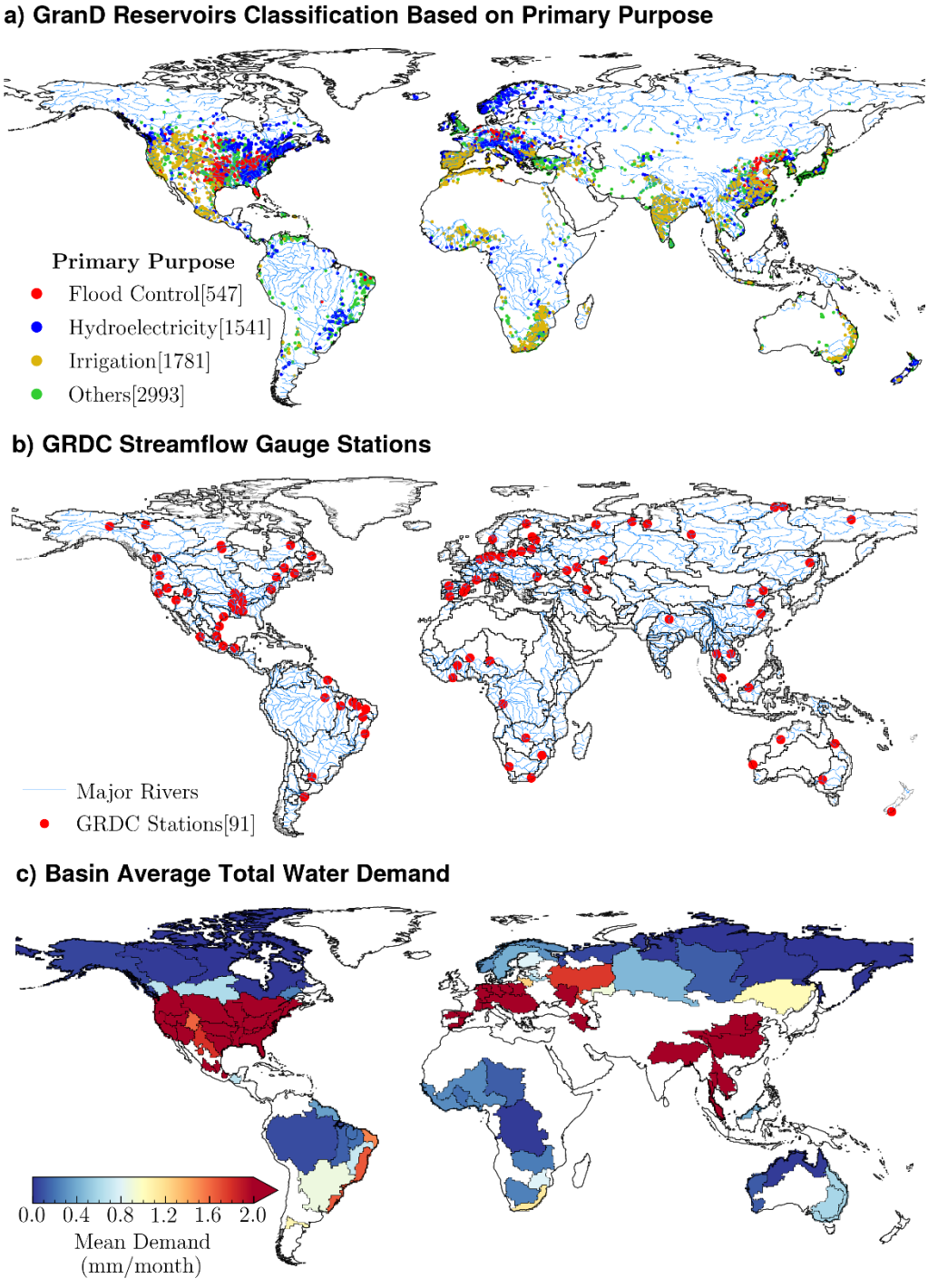

Figure 3: Global data used in this study: (a) Global distribution of 6862 reservoirs from the GRanD database classified based on primary reservoir purpose; (b) GRDC stream gauge stations in 91 basins where data were of sufficient length, quality, and upstream watershed contributing area for use in this study; and (c) basin mean monthly water demand in those same 91 river basins.

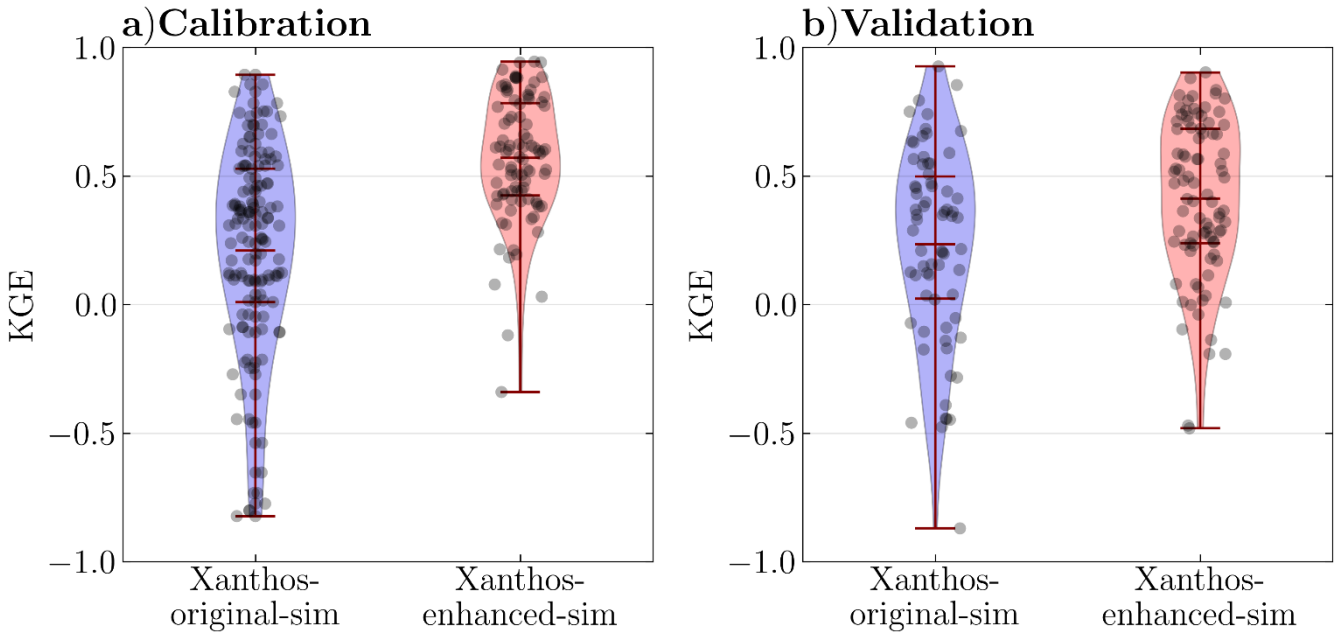

Figure 4: Boxplots of the KGE values for the *Xanthos-original-sim* and *Xanthos-enhanced-sim* simulations during: (a) the calibration period (1971-1980) and (b) the validation period (1981-1990). In this plot, the outliers (KGE values lower than -1) are not shown. For *Xanthos-original-sim*, 77 basins in calibration and 70 basins in validation are shown, and for *Xanthos-enhanced-sim*, 91 basins during calibration and 89 during validation are shown.

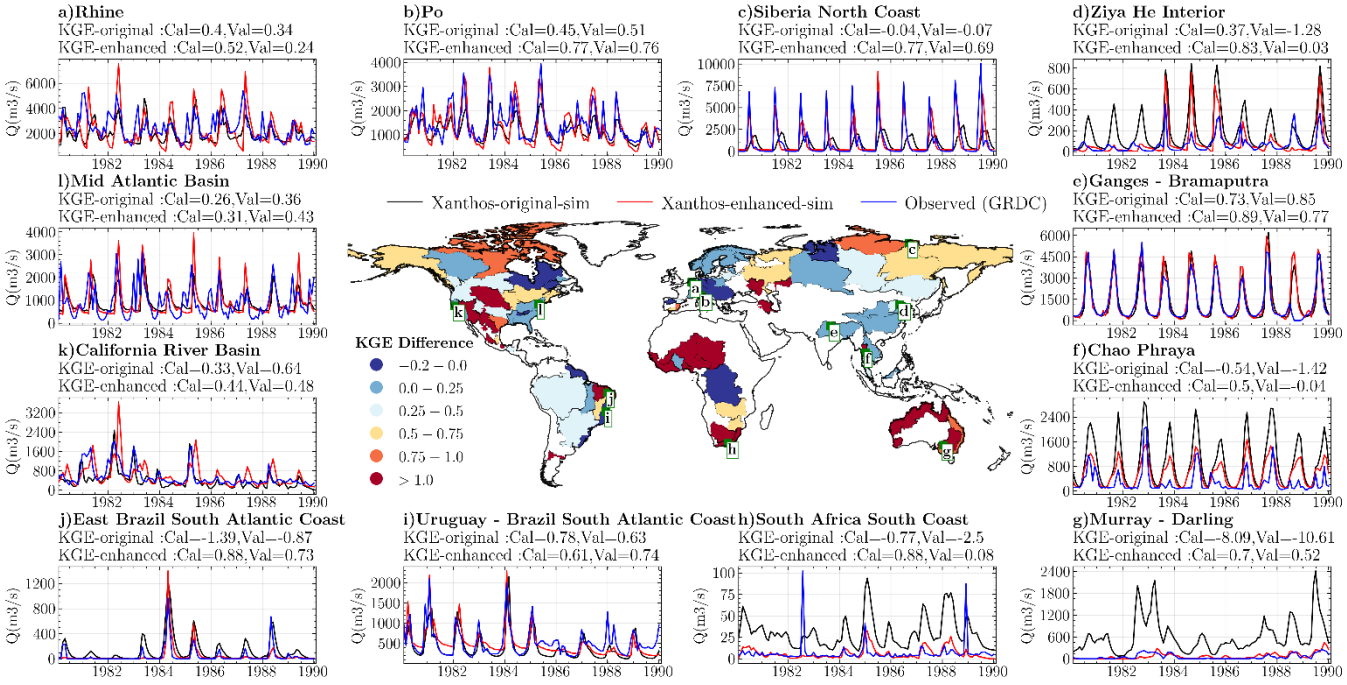

Figure 5: Spatial maps of basin-specific difference between the KGE values from *Xanthos-enhanced-sim* and those from *Xanthos-original-sim* for the calibration period 1971-1980 (map at center), where greater than zero indicates improved performance from the addition of water management features to Xanthos. The time series plots are simulated and observed monthly streamflow for basins with the highest water demand in different global regions during the validation period (1981-1990). *KGEcal* is the KGE during the calibration period, while *KGEval* is the KGE during the validation period.

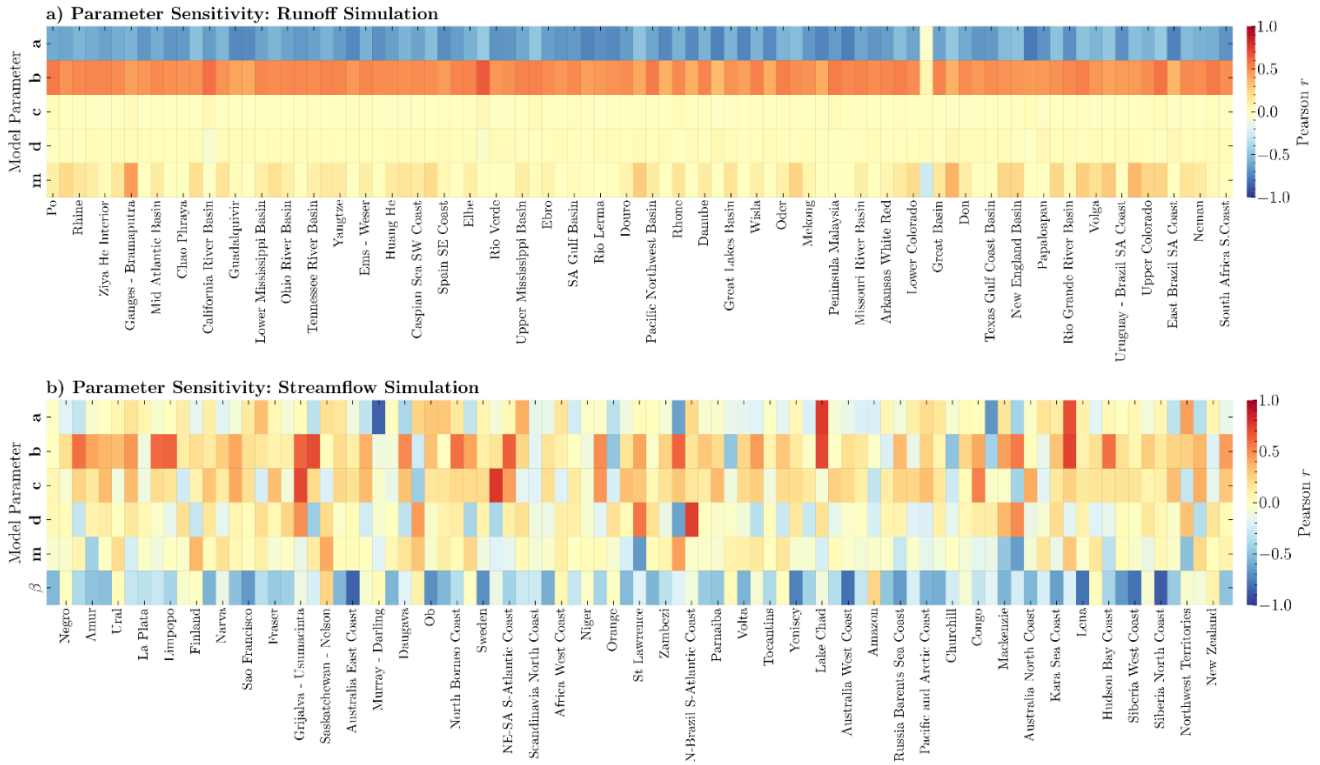

Figure 6: Parameter sensitivity analysis for *Xanthos-enhanced* in the form of the Pearson correlation coefficient (Pearson r): (a) between runoff parameters (i.e., 1 million parameter sets) and their corresponding Normalized Root Mean Squared Error (NRMSE) computed with annual runoff, (b) between streamflow simulation parameters (i.e., the combination of the top 100 runoff parameter sets and sampled routing parameter) and KGE computed from streamflow simulated at monthly scale. A higher Pearson r implies that the model performance is more sensitive to the parameter. For instance, for (a) Pearson r less than zero indicates a decrease in annual runoff NRMSE as parameter value increases, while Pearson r greater than zero indicates a positive association between annual runoff NRMSE and parameter value. Note: Out of the 91 basins, only half of the basin labels (i.e., the x-axis labels) appear on the first panel, and the other half appears on the second panel, but all labels apply to both panels.

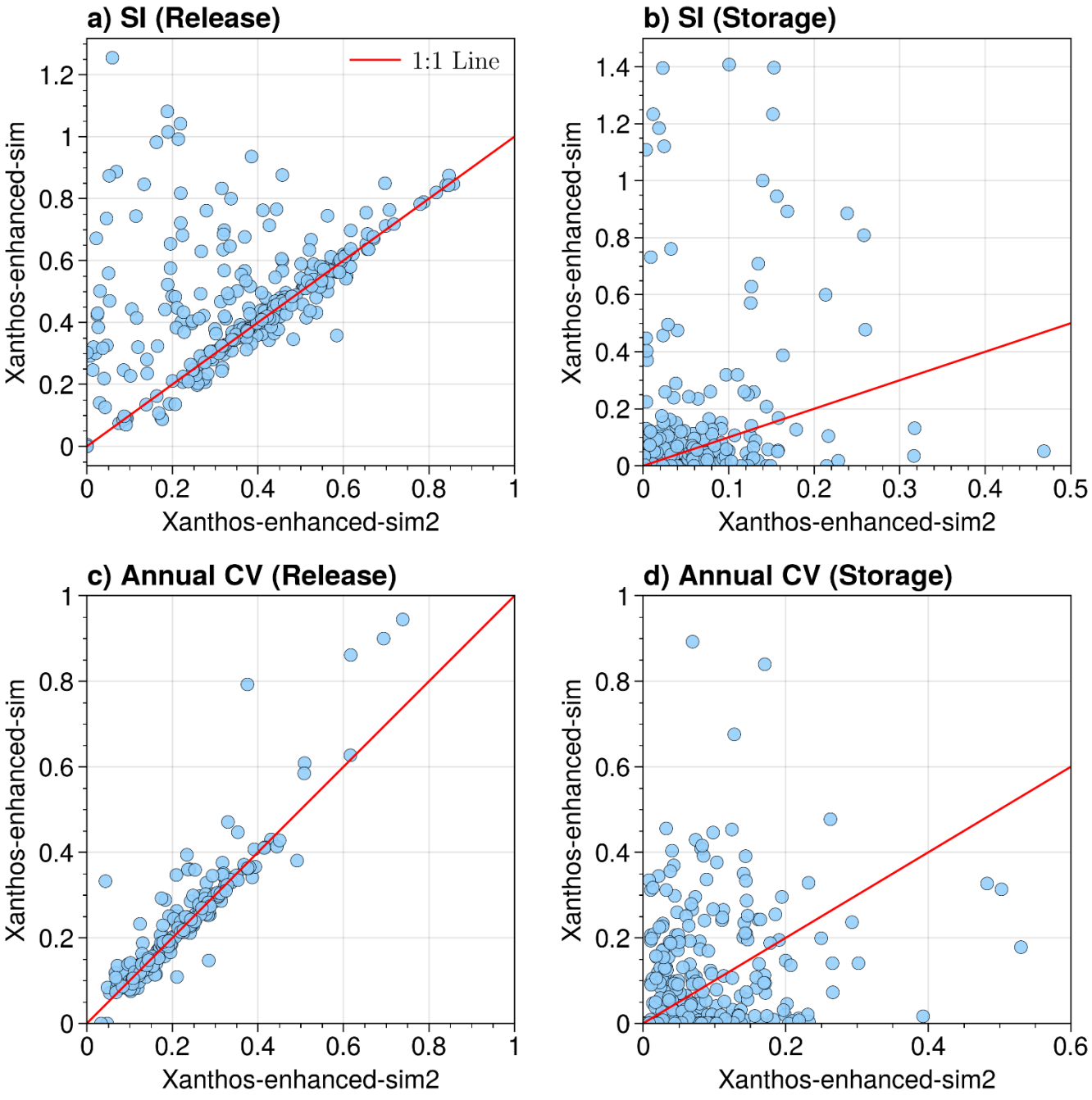

Figure 7: Comparing intra-annual and inter-annual variability of storages and releases simulated with *Xanthos-enhanced-sim* and *Xanthos-enhanced-sim2* experiments hydropower reservoirs distributed over the 91 basins. a) Seasonality Index (SI) for release, b) Seasonality Index for storage, c) Coefficient of Variation (CV) for release at the annual scale, and d) Coefficient of Variation (CV) for storage at the annual scale. The red line is a 1:1 line where both scenarios are equal.

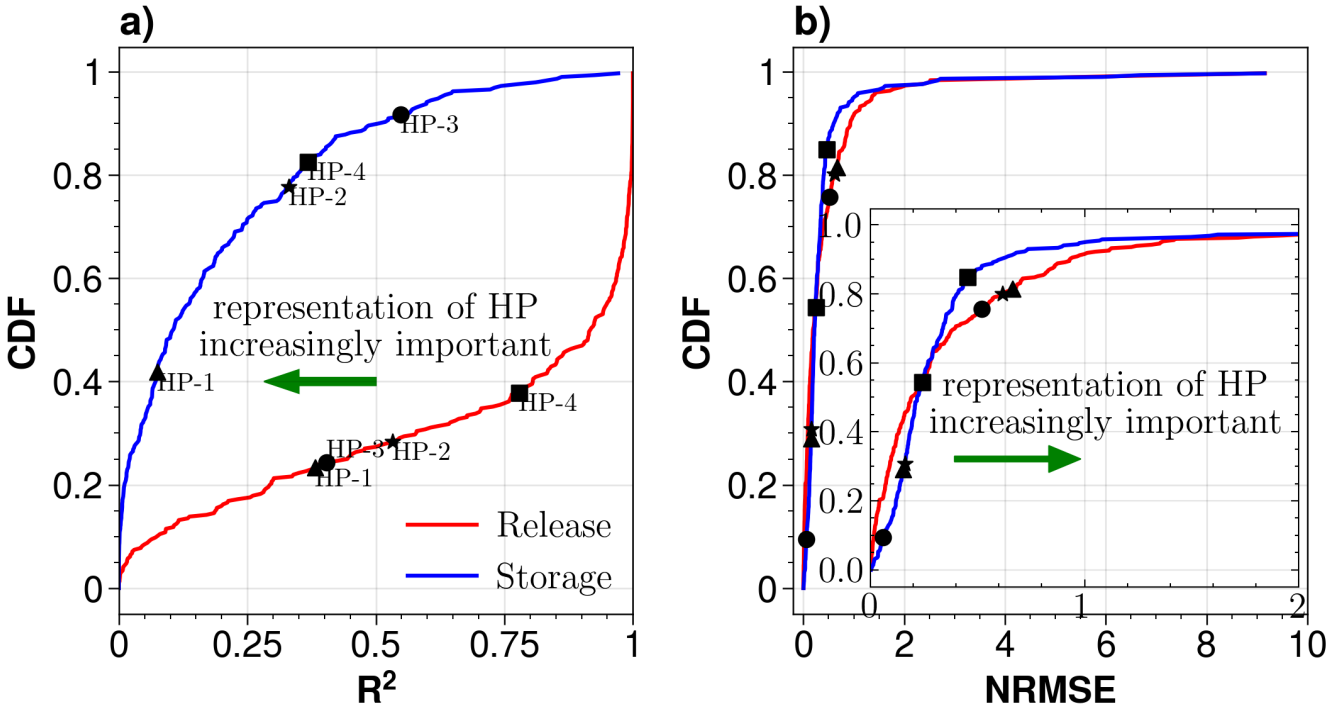

Figure 8: Empirical CDF of reservoir storage and release R^2 (a) and NRMSE (b) between *Xanthos-enhanced-sim* and *Xanthos-enhanced-sim2* monthly simulations across all hydropower reservoir sites. The R^2 CDF plot demonstrates that we produce very different storage and release patterns by accounting explicitly for hydropower reservoir functionality in *Xanthos-enhanced-sim*, although the difference in magnitude, as indicated by NRMSE CDF, is small. A higher R^2 of 1.0 and NRMSE of 0.0 represent a perfect agreement between the two simulations, indicating that distinguishing between the representation of hydropower and flood control behavior was less important for basins with those values. The CDF plot is made of 296 hydropower reservoirs distributed across 51 basins. The labels on plots HP-1, HP-2, HP-3, and HP-4 correspond to hydropower reservoirs located upstream of the Yenisey basin's GRDC site (see supplementary Fig. S5), discussed in Section 3.5. The markers for these labels are similar for both a) and b).

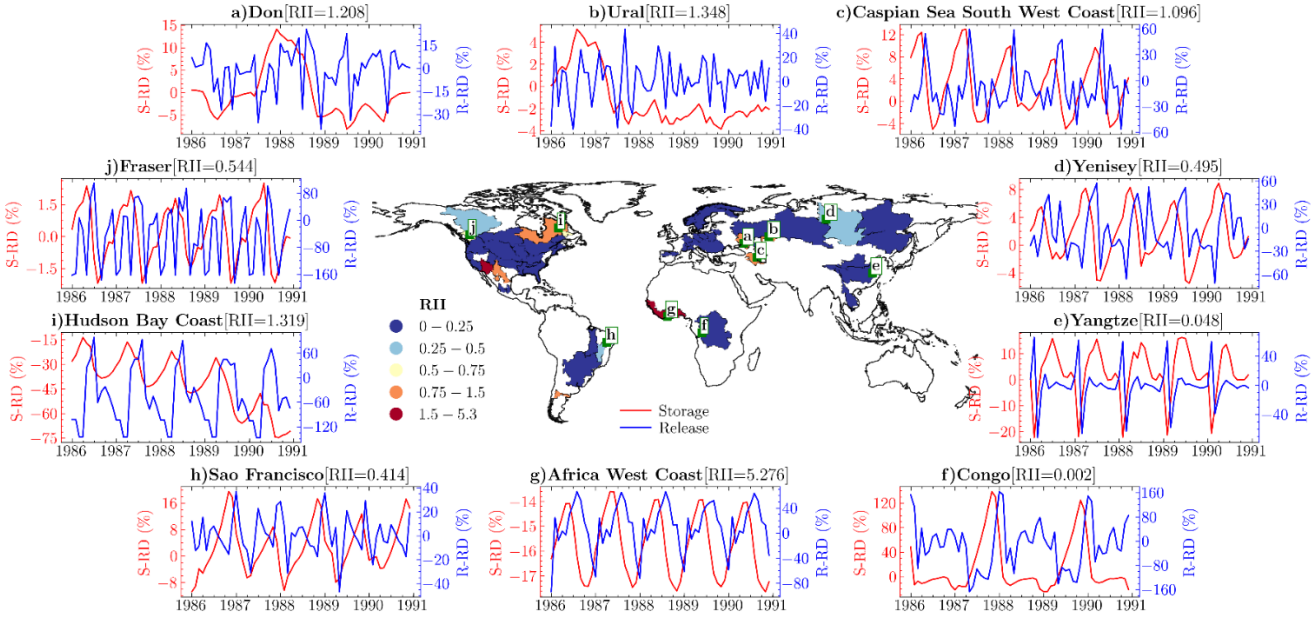

Figure 9:The difference between reservoir storage and release monthly time series between *Xanthos-enhanced-sim* and *Xanthos-enhanced-sim2* simulations at hydropower reservoirs demonstrates the value-added by accounting explicitly for hydropower reservoir functionality in *Xanthos-enhanced-sim*. The Reservoir Impact Index (RII) is the ratio of reservoir storage capacity (in cubic meters) to annual mean flow(in cubic meters). Low and high values of RII indicate that the stream is lightly and highly regulated, respectively. For instance, RII > 1.0 shows the reservoir's capacity to shift the downstream flow below the annual mean flow. The map at the center of the figure displays the RII for the hydropower reservoir with the largest RII in each basin. In other words, each basin is represented by one hydropower reservoir with the largest impact on flow at the GRDC site. The times series plots show the Storage Relative Difference (S-RD) and Release Relative Difference (R-RD) between the two scenarios. For example, S-RD represents *Xanthos-enhanced-sim* storage minus *Xanthos-enhanced-sim2* storage scaled by the mean of the two storages.

Supplementary Figures

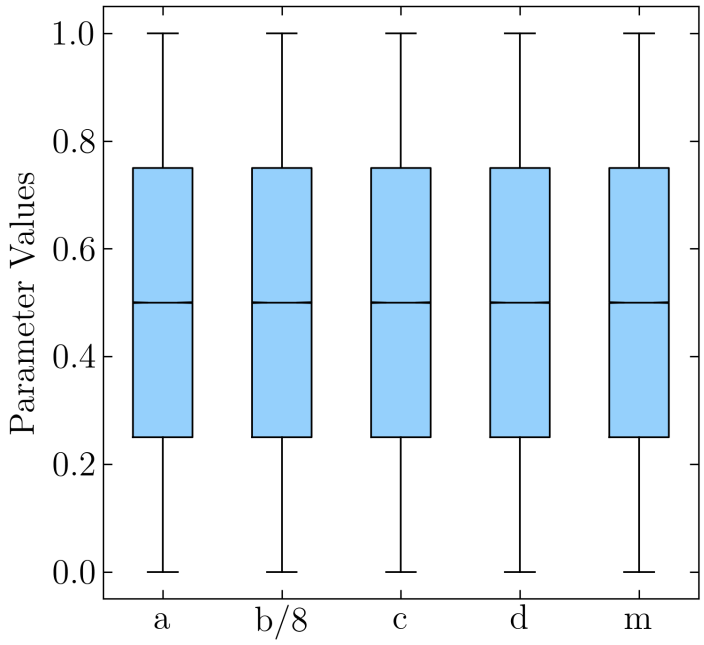

Figure S1: Sampling runoff generation parameters using the Latin Hypercube Sampling (LHS) method. Parameter b ranges between 0-8 meters, and it is scaled by 8 (b/8) for plotting purposes.

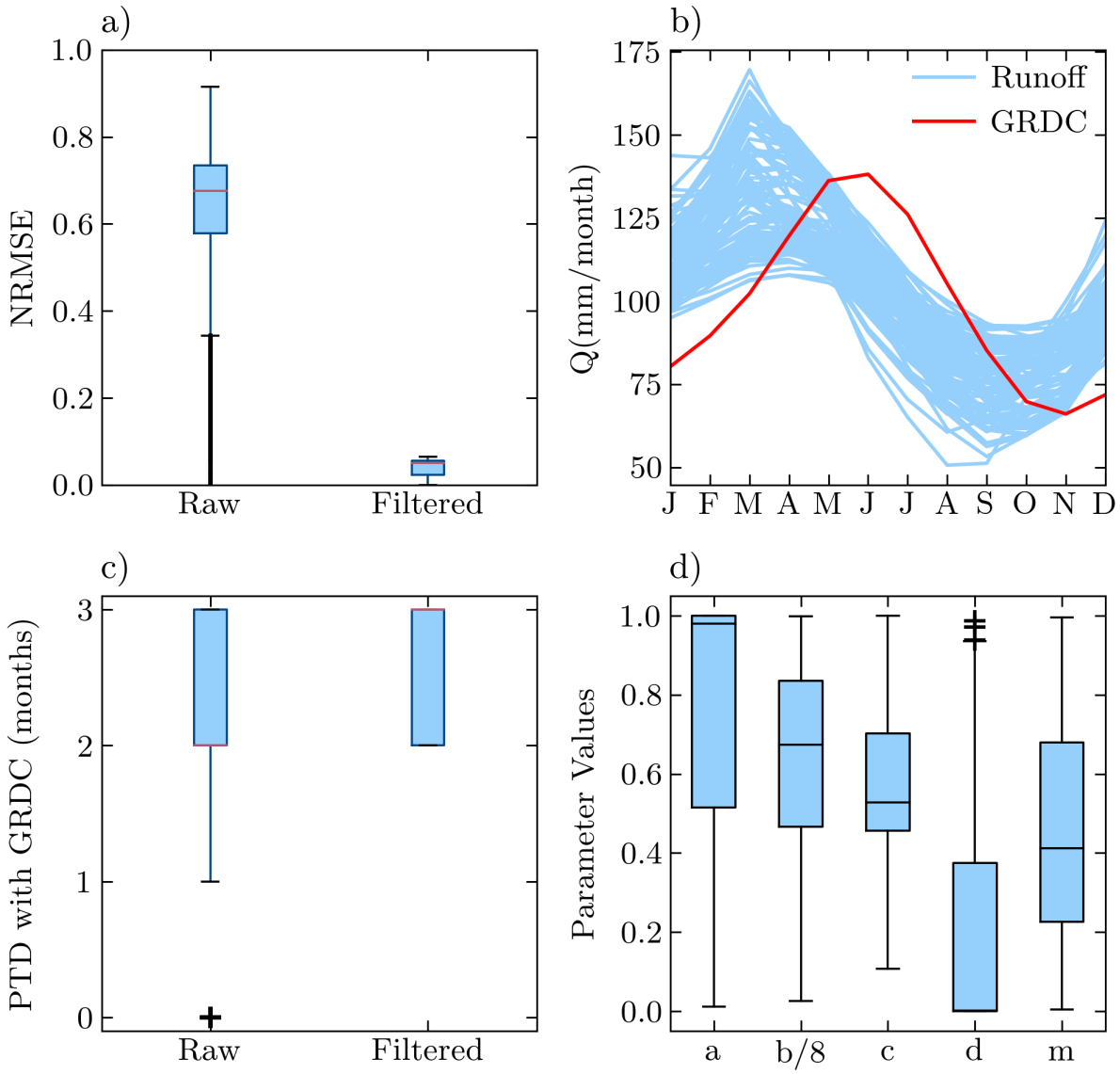

Figure S2: First-stage parameter determination over the Amazon River basin: (a) NRMSE between simulated annual runoff and observed annual streamflow time series for original one million parameter sets (raw) and the selected subset of one hundred parameter sets (filtered), (b) Mean monthly runoff corresponding to the selected top 100 (filtered) parameters and observed mean monthly streamflow from the GRDC station, (c) Peak Time Difference (PTD), the difference between the average peak runoff time (month) and peak flow time for the raw and filtered parameter sets, and (d) distribution of the parameter values from the 100 selected parameter combinations after filtering. Parameter b is normalized by 8 for plotting along with the other parameters.

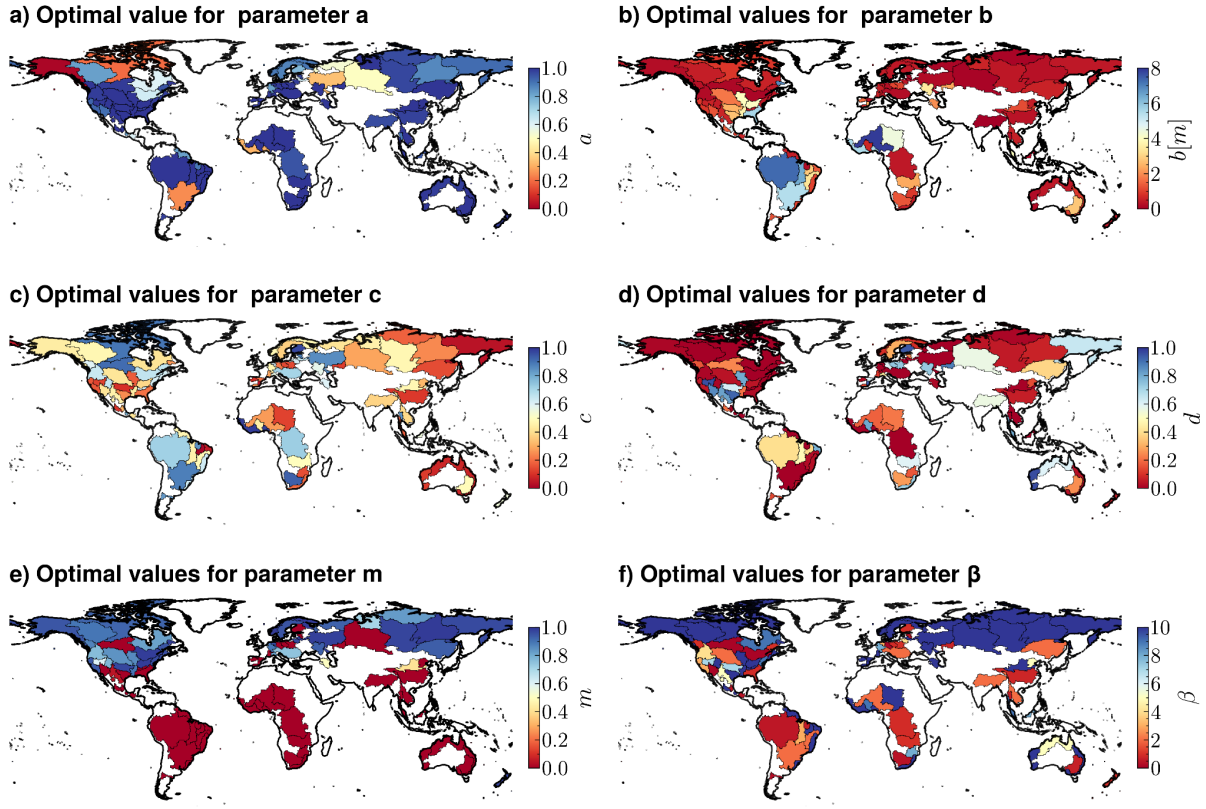

Figure S3: Spatial maps of the final parameter values after the 2nd-stage parameter determination. See Table 2 for a description of the parameter values.

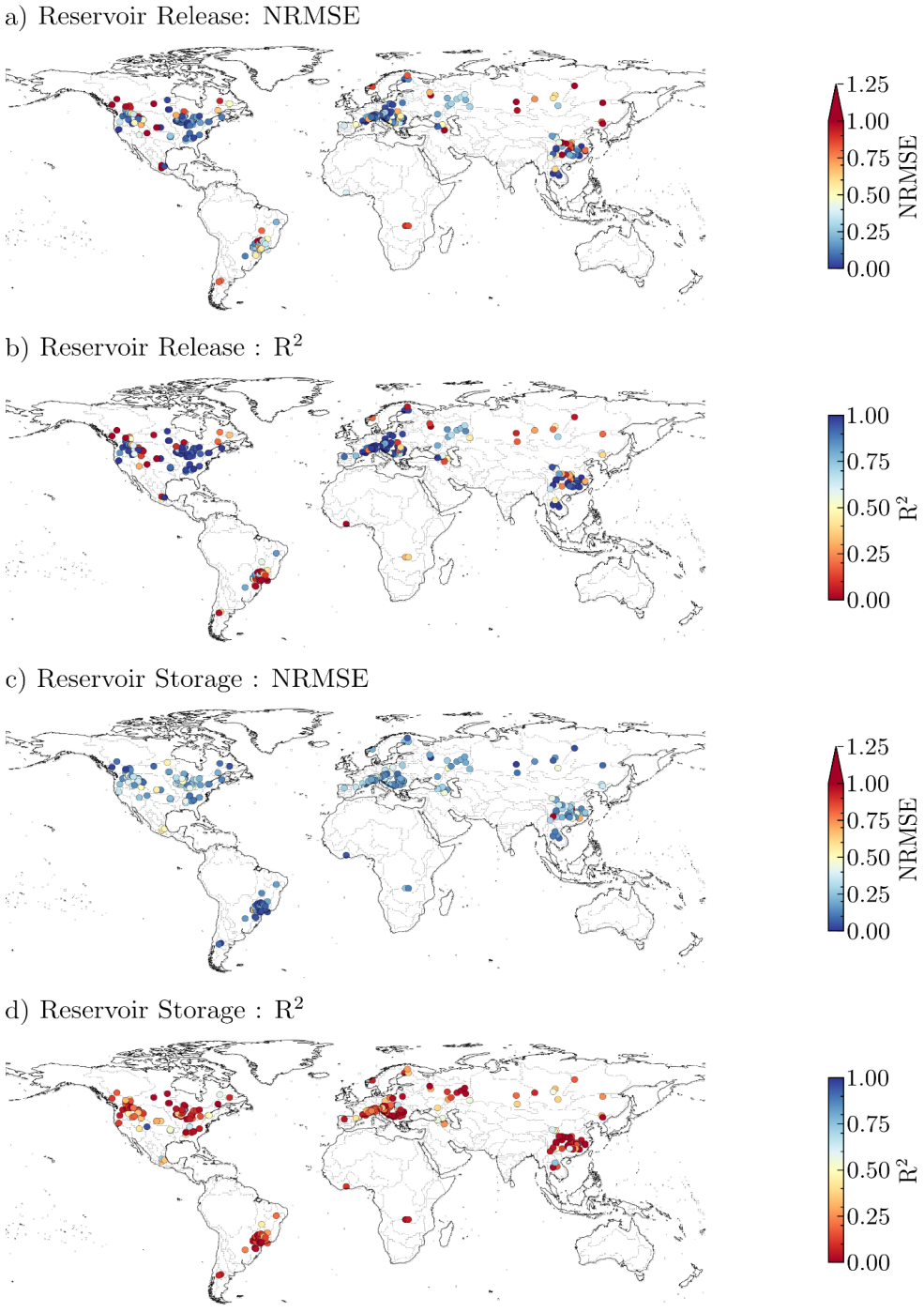

Figure S4: The difference between reservoir storage and release time series between Xanthos-enhanced-sim and Xanthos-enhanced-sim2 simulations at hydropower reservoirs demonstrates the value-added by accounting explicitly for hydropower reservoir functionality in *Xanthos-enhanced-sim*. A higher R^2 of 1.0 and NRMSE of 0.0 indicate a perfect agreement between the two.

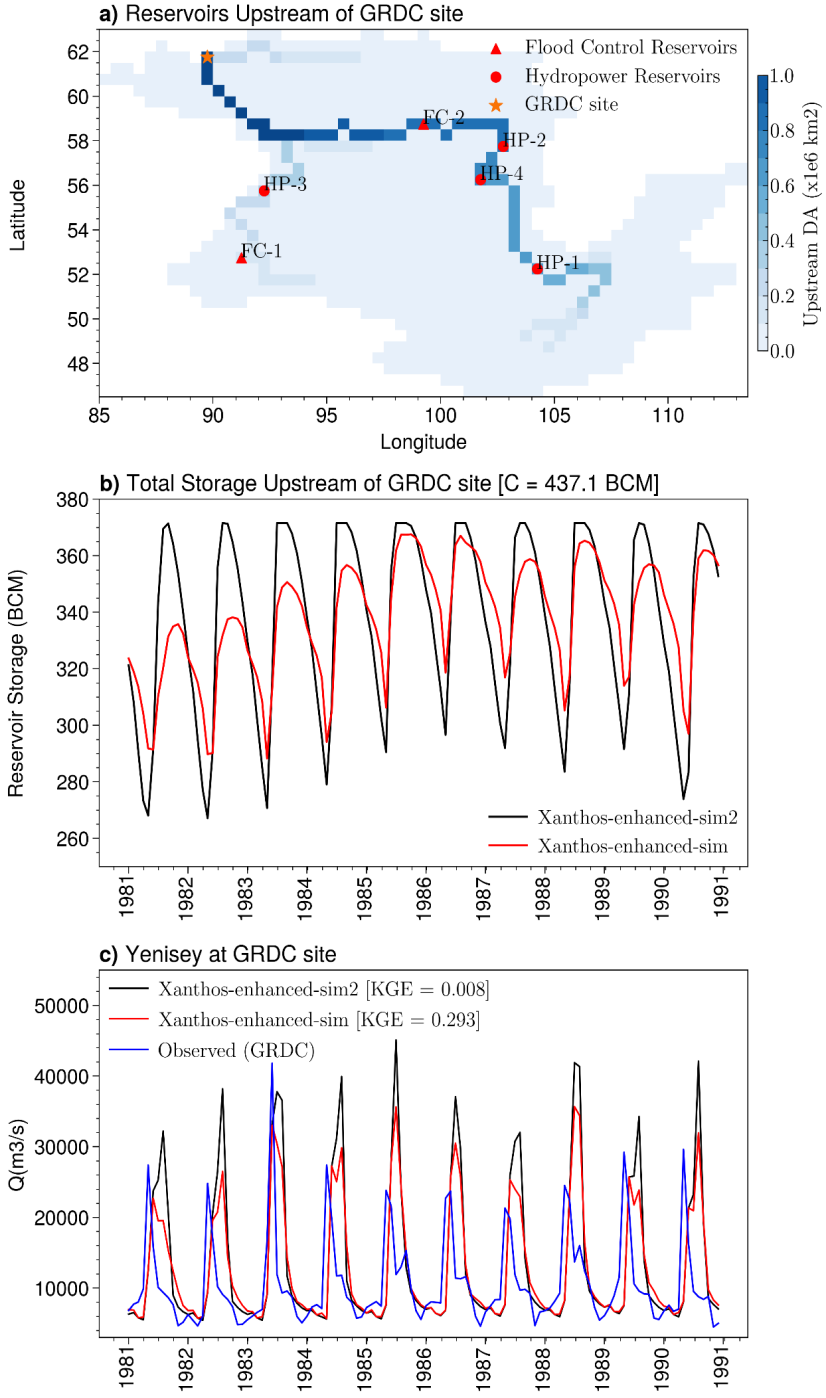

Figure S5: Yenisey basin: (a) reservoir distributions upstream of the GRDC site, (b) total reservoir storage upstream of the GRDC site, and (c) streamflow at the GRDC site. Upstream DA is the upstream drainage area, and C is the total capacity of reservoirs upstream of the GRDC site.

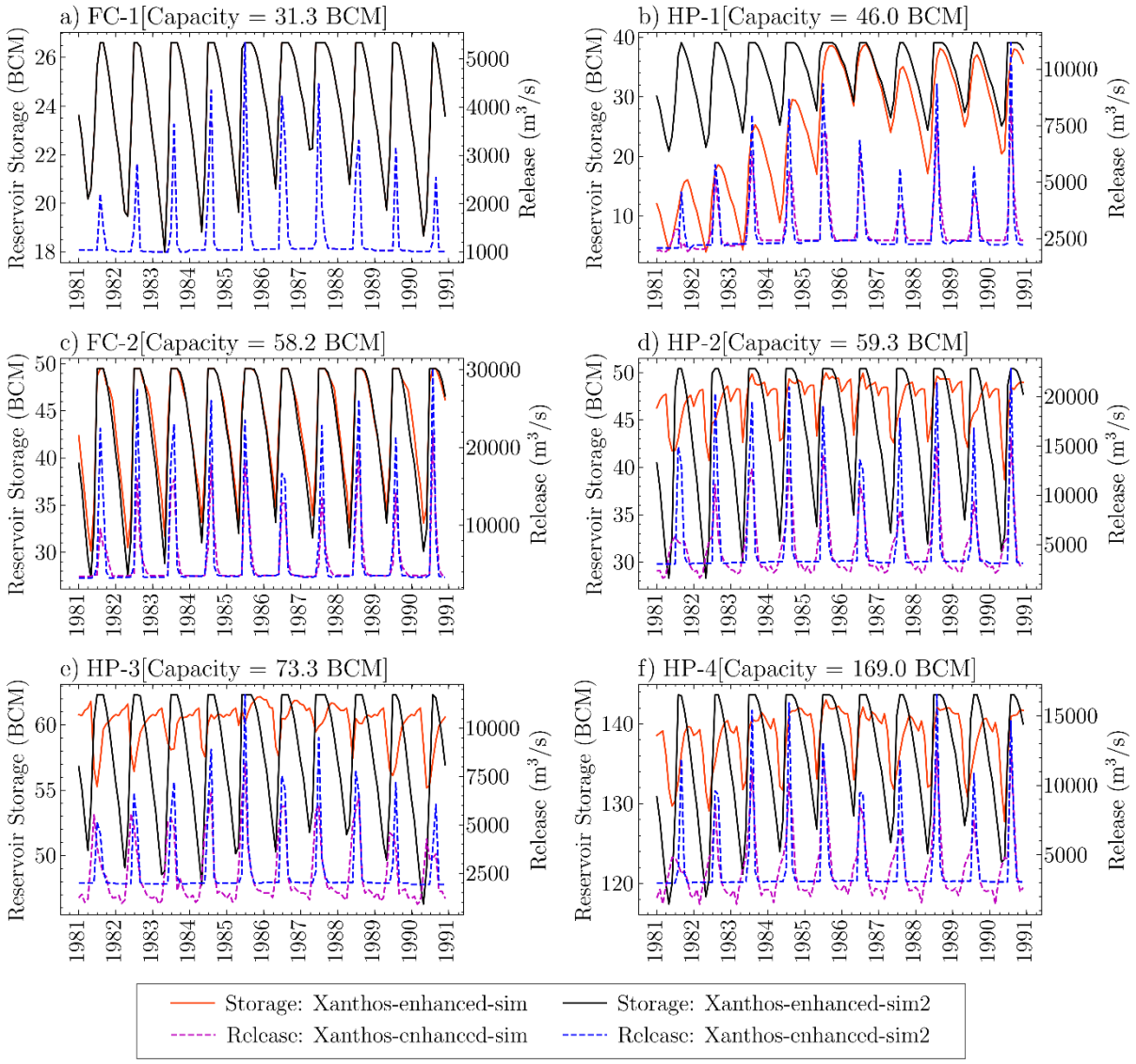

115 **Figure S6: Simulated storage and release characteristics for reservoirs located upstream of Yenisey basin GRDC station for the last ten years of our simulation. Four are hydropower (a, d, e, and f), and two are flood control (b and c) reservoirs. The reservoirs are arranged from (a) – (f) in order of increasing storage capacity.**

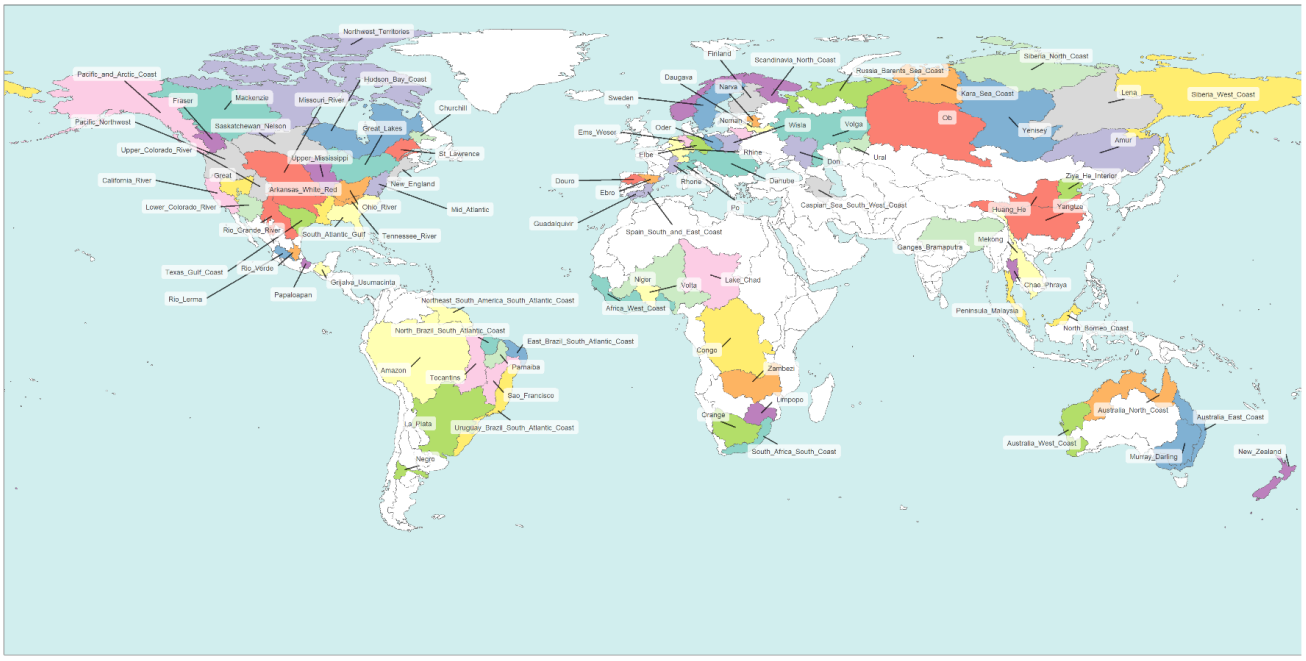

Figure S7: The 91 Xanthos basins calibrated in this study with basin name label

120